

**Calcineurin orchestrates lateral transfer of *Aspergillus fumigatus* during macrophage cell death**

Anand Shah<sup>1\*</sup>, Shichina Kannambath<sup>1\*</sup>, Susanne Herbst<sup>1</sup>, Andrew Rogers<sup>2</sup>, Simona Soresi<sup>3</sup>, Martin Carby<sup>3</sup>, Anna Reed<sup>3</sup>, Serge Mostowy<sup>4</sup>, Matthew C. Fisher<sup>5</sup>, Sunil Shaunak<sup>6</sup>, Darius P. Armstrong-James<sup>1+</sup>

1 National Heart and Lung Institute, Imperial College London, London SW7 2AZ UK

2 Histopathology Department, Royal Brompton and Harefield Hospitals, London SW3 6NP UK

3 Lung Transplant Unit, Royal Brompton and Harefield Hospitals, Middlesex, UB9 6JH UK

4 MRC Centre for Molecular Bacteriology and Infection, Imperial College London, London SW7 2AZ UK

5 School of Public Health, Imperial College London, London W2 1PG UK

6 Department of Infectious Diseases and Immunity, Imperial College London, London W12 0NN UK

\* These authors contributed equally

+ Corresponding Author

Tel: +44207 594 3187

Email: [d.armstrong@imperial.ac.uk](mailto:d.armstrong@imperial.ac.uk)

Fax: unavailable

Address: Fungal Pathogens Laboratory, National Heart and Lung Institute, Sydney Street Wing, Royal Brompton Hospital, London UK SW3 6NP

**Impact:** Pulmonary aspergillosis is a life-threatening complication in transplantation and chronic respiratory disease. Here we report necroptosis as an early response to germination of *Aspergillus fumigatus* in human macrophages, and show that this results in lateral transfer of *Aspergillus fumigatus* between macrophages as a mechanism to limit hyphal escape. We define calcineurin as a key phosphatase that regulates necroptotic transfer of *Aspergillus fumigatus*, yielding important insights into the pathogenesis of pulmonary aspergillosis in the immunocompromised host.

**Author contributions:** D.A-J, A.S., S.K., S.S. and S.M. designed the experiments. D.A-J, A.S, S.K., S.H., and A.Ro. conducted the experiments. S.S, A.Re. and M.C. consented the patients and undertook the bronchoscopies. A.S. and S.K. wrote the first draft of the manuscript. All authors contributed to the data analysis and the writing of the manuscript.

**Funding:** This work was supported by an MRC Clinician Scientist Fellowship to DAJ [G0902260/1] and an MRC Clinical Research Fellowship [MR/K002708/1] to AS. SM is supported by a Wellcome Trust Research Career Development Fellowship [WT097411MA] and by the Lister Institute for Preventative Medicine.

**Running Head:** Macrophage necroptosis in pulmonary aspergillosis

**Descriptor number:** 10.6 Host Defenses to Microbial Pathogens

**Manuscript word count:** 3442/3500

**At a Glance Commentary**

**Scientific Knowledge on the Subject:** Macrophages are the front-line defense against pulmonary infection with the mould pathogen *Aspergillus fumigatus*. Phagocytosis and generation of reactive oxygen species are known to be crucial for control of infection. However, the cellular outcome from progressive macrophage infection with *Aspergillus fumigatus* has not been systematically studied.

**What This Study Adds to the Field:** Here we present a systematic analysis of human macrophage infection with *Aspergillus fumigatus*. We show that successful fungal germination in the phagosome leads to necrotic cell death and can result in cell-cell transfer of germinating *Aspergillus fumigatus* between macrophages. Ultimately this process assists control of fungal germination, and is orchestrated through the calcium-responsive serine-threonine phosphatase calcineurin. Our systematic analysis of the macrophage response to *Aspergillus fumigatus* defines necroptosis as a key early event in the pathogenesis of pulmonary aspergillosis.

**This article has an online data supplement, which is accessible from this issue's table of content online at [www.atsjournals.org](http://www.atsjournals.org)**

## Abstract

**Rationale:** Pulmonary aspergillosis is a lethal mould infection in the immunocompromised host. Understanding initial control of infection, and how this is altered in the immunocompromised host, is a key goal for understanding the pathogenesis of pulmonary aspergillosis.

**Objectives:** To characterise the outcome of human macrophage infection with *Aspergillus fumigatus*, and how this is altered in transplant recipients on calcineurin inhibitor immunosuppressants.

**Methods:** We defined the outcome of human macrophage infection with *Aspergillus fumigatus*, and the impact of calcineurin inhibitors, through a combination of single cell fluorescence imaging, transcriptomics, proteomics, and *in vivo* studies.

**Measurements and Main results:** Macrophage phagocytosis of *Aspergillus fumigatus* enabled control of 90% of fungal germination. However fungal germination in the late phagosome led to macrophage necrosis. During programmed necroptosis, we observed frequent cell-cell transfer of *Aspergillus fumigatus* between macrophages which assists subsequent control of germination in recipient macrophages. Lateral transfer occurred through actin-dependent exocytosis of the late endosome in a vasodilator-stimulated phosphoprotein (VASP) envelope. Its relevance to the control of fungal germination was also shown by direct visualisation in our zebrafish aspergillosis model *in vivo*. The calcineurin inhibitor FK506/tacrolimus reduced cell death and lateral transfer *in vitro* by 50%. This resulted in uncontrolled fungal germination in macrophages and hyphal escape.

**Conclusions:** These observations identify programmed necrosis-dependent lateral transfer

of *Aspergillus fumigatus* between macrophages as an important host strategy for controlling fungal germination. This process is critically dependent on calcineurin. Our studies provide fundamental insights into the pathogenesis of pulmonary aspergillosis in the immunocompromised host.

**Word count:** 248

**Key Words:** Pulmonary Fungal Diseases; Macrophage; Necrosis; Aspergillus; Calcineurin

## Introduction

*Aspergillus fumigatus* (*Af*) is a mould with small airborne conidia that are a ubiquitous component of the aerial mycobiota (1). Normally inhaled conidia are cleared by alveolar macrophages to prevent fungal germination, tissue invasion and destructive lung disease (2, 3). Our previous work using murine and zebrafish models of invasive aspergillosis has shown the importance of macrophages in control of *Af* early post infection, with neutrophil influx a later event (4, 5). Previous studies have highlighted the importance of inflammatory monocytes in murine invasive aspergillosis (6).

A spectrum of immunocompromised states predispose individuals to high-mortality invasive or chronic forms of pulmonary aspergillosis (PA) (7). Organ transplant recipients are at high risk of PA, with lung transplant recipients being particularly susceptible with a mortality of >40% (8, 9). There are an estimated 3 million individuals with chronic PA, and 4.5 million with allergic bronchopulmonary aspergillosis globally (10, 11). *Af* has also been implicated in the pathogenesis of asthma, chronic obstructive airways disease and bronchiectasis (11-13). Treatment options remain limited, and high mortality rates persist (14). Better understanding of susceptibility to PA in the non-neutropenic host is a key clinical research priority.

Calcineurin-NFAT signalling is the target of the calcineurin inhibitor immunosuppressants (CNIs) used in organ transplantation (15). We have shown that CNIs (FK506/tacrolimus) increase susceptibility to murine PA through inhibition of the macrophage TLR9-calcineurin-NFAT pathway (4, 5). This pathway is crucial for activation of inflammatory responses to *Af*, and recruitment of fungicidal neutrophils to the site of infection. Calcineurin-NFAT signalling has also been shown to be critical for the innate immune response to *Candida albicans* and

*Escherichia coli*, through endocytic mechanisms convergent on phospholipase C- $\gamma$ -dependent calcium flux (16, 17). These observations underscore the importance of calcineurin-NFAT signalling for myeloid immunity, and reveal a novel relationship between innate sensing and calcineurin-NFAT signalling in the lung that requires further clinical definition.

Here we show that host programmed necrosis is an important outcome of *Af* germination in the human macrophage. Cell death occurred in response to phagosomal germination, with necroptosis-associated lateral transfer of *Af* between macrophages. Cell death-dependent transfer was calcineurin-dependent, and enabled control of germination in recipient macrophages. Crucially, inhibition of either calcineurin-dependent cell death, or lateral transfer, enabled hyphal escape from the macrophage. These studies identify programmed necrosis as a key cellular response in PA, and show that it is likely to be critically impaired in organ transplant recipients on calcineurin inhibitors. Our studies reveal cell-cell transfer as a novel and important cell death associated defence mechanism that enables control of fungal germination in the myeloid compartment.

## Methods

## Ethics Statement

Studies were approved by the Biomedical Research Unit (NRES reference 10/H0504/9), Royal Brompton and Harefield NHS Trust (AS1). All experiments conformed to the WMA declaration of Helsinki. Written informed consent was obtained from all participants.

### **Zebrafish care and maintenance**

Experiments were approved by the United Kingdom Home Office in accordance with the project license PPL 70/7446. Full details are given in the Supplemental Experimental Procedures.

### **Fungal strains and culture**

*A. fumigatus* CEA10 was used for Western blot, Luminex, fungal burden, Imagestream, phosphoproteomic and RNA sequencing experiments. ATCC46645-eGFP, a gift from Frank Ebel, was used for microscopy experiments. See Supplemental Experimental Procedures.

### **Isolation of human macrophages**

hAMs were isolated from bronchoalveolar lavage by adherence. Purified hAMs were rested for 3 days. Monocytes were isolated from peripheral blood mononuclear cells (PBMCs) from healthy volunteers by Ficoll-Paque gradient centrifugation and negative magnetic bead isolation (Pan-monocyte isolation kit, Miltenyi Biotec, CA, USA). hMDMs were differentiated using 5ng/ml granulocyte-macrophage colony-stimulating factor (GM-CSF) and 10% human serum for 7 days. See Supplemental Experimental Procedures.

### **RNA-seq analysis**

Illumina RNA-seq libraries were prepared from hMDMs ( $n = 6$ , healthy donors) pre-treated with 10 ng/ml FK506 for 1h or vehicle and stimulated with live *Af* swollen conidia (SC) (MOI=1) for 1h and 6h. Illumina paired-end reads were mapped to the human reference genome (hg19) using TopHat2 (18) (GEO database accession number GSE74924) and differential expression analyses performed using Cufflinks v2.2.1 (19). Gene analyses were carried out using DAVID v6.7 (20). Human PPI network modules were obtained using MCODE (21) analysis in Cytoscape. See Supplemental Experimental Procedures.

### **Phosphoproteomic analysis**

A Phospho Explorer Antibody Microarray was conducted by Full Moon BioSystems Inc (California, USA). hMDMs were differentiated at  $1 \times 10^7$  cells in 75mm<sup>2</sup> tissue culture flasks. At day 7, cells were stimulated with live *Af* swollen conidia (SC) (MOI=1) following pre-treatment for 1h with FK506 (10ng/ml, Calbiochem) or vehicle (DMSO diluted in RPMI). At 1h post-infection, cells were washed (x5) with 10mls ice-cold phosphate-buffered saline (PBS) containing protease inhibitors (Cell Signalling), and collected by centrifugation (250g for 10min at 4°C). Cells were frozen at -80°C and transferred to Full Moon Biosystems on dry ice. The array consisted of 1,318 phospho-specific antibodies. Proteins were labelled with biotin and adhered to pre-blocked microarray slides. After washing, detection of total and phosphorylated proteins was conducted using Cy3-conjugated streptavidin. Expression of phosphorylated proteins was normalized to the corresponding total protein abundance. Fold change was calculated as the phospho- to non-phospho-protein ratio of FK506-treated cells/the phospho- to non-phospho-protein ratio of untreated cells.

### **Statistical analysis**

Results are presented as mean  $\pm$  SEM and were analyzed using GraphPad Prism software (version 6.0; GraphPad). Significance was determined using a Student's *t* test for unpaired observations; \**P*  $\leq$  0.05; \*\**P*  $\leq$  0.01; \*\*\**P*  $\leq$  0.001. If 3 or more groups were compared a one-way ANOVA with Bonferroni correction was used.

Full details of Experimental Procedures are available in the Supplemental Information.

## Results

### ***Aspergillus fumigatus* activates calcineurin-NFAT-dependent inflammatory responses in human macrophages**

*Af* phagocytosis activates NFAT nuclear translocation in murine macrophages (4). We therefore characterised the role of NFAT in human monocyte-derived macrophages (hMDMs). hMDMs were infected with live *Af* swollen conidia (SC) or resting conidia (RC) and NFAT translocation determined by Western blot and confocal microscopy. SC phagocytosis led to sustained NFAT translocation after 30min (Figures 1A, B and E1A). RC induced a weak transient NFAT activation response (Figure E1B, E1C). NFAT translocation in response to SC was confirmed in alveolar macrophages (hAMs) from lung transplant recipients (Figure E1D). Maximum translocation of NFATc2 to the nucleus was seen in response to *Af* at 60 minutes p.i. NFAT translocation was blocked by the calcineurin inhibitor FK506 (Figures 1B, 1C, E1E), but NF $\kappa$ B Rel65 translocation was unaffected (Figure 1B).

NFAT transcriptional activity was defined by measuring expression of the NFAT-specific target Regulator of Calcineurin 1 (*RCAN1*). SC infection increased *RCAN1* expression, which was abrogated by FK506 (Figures 1D, E1F). To determine the role of the calcineurin-NFAT pathway in inflammatory responses, we quantified chemokine and cytokine production in hMDMs during SC infection. *TNF- $\alpha$* , *GM-CSF*, *MCP-1*, *MCP-1 $\alpha$*  and *MCP-1 $\beta$*  expression were attenuated by calcineurin inhibition ( $P=0.02$ ;  $P=0.02$ ;  $P=0.03$ ;  $P=0.0003$  and  $P=0.009$  respectively) (Figures 1E, E1G). Flow cytometry characterisation of hMDMs and lung transplant hAMs revealed similar inflammatory activation status with CD11c<sup>+</sup>MHCII<sup>+</sup>CD206<sup>+</sup> surface expression. There were significant differences in surface CD11b ( $P\leq 0.001$ ) and CD86 ( $P\leq 0.001$ ) expression (Figure E1H). Blockade of the fungal C-type lectin receptor Dectin-1 ( $P=0.001$ ) or inhibition of downstream Syk signalling ( $P=0.001$ ) impaired TNF- $\alpha$  responses, but there was no effect on NFAT translocation (Figures E1I, E1J). These results indicate that the calcineurin-NFAT signalling pathway is critical for early macrophage inflammatory responses to *Af*, independent of Dectin-1 and Syk, in humans.

#### **Human macrophage phagocytosis, reactive oxygen species production and killing of *A. fumigatus* are calcineurin-dependent**

Next we characterised the role of calcineurin-NFAT in killing of *Af*. hMDMs were infected with SC following treatment with FK506 or vehicle, and fungal growth analysed at 1 and 6h p.i.. Both hMDMs and hAMs pre-treated with FK506 exhibited impaired control of fungal growth ( $P<0.001$  and  $P<0.0001$  respectively) (Figures 2A, E2A). Time-lapse video microscopy demonstrated increased *Af* hyphal transition in FK506-treated macrophages ( $P=0.02$ ) (Figure 2B). To identify the calcineurin-dependent mechanism for fungal growth inhibition, we assessed efficiency of *Af* phagocytosis. Calcineurin inhibition delayed phagocytosis of SC in

hMDMs ( $P<0.01$ ) and hAMs ( $P=0.04$ ) early post-infection but phagocytosis of RC was not affected (Figures 2C, E2B, E2C). We measured reactive oxygen species (ROS) production and Cathepsin B (a lysosomal cysteine protease) activation, which are critical for *Af* killing (22, 23). ROS production was partially calcineurin-dependent ( $P<0.0001$ ) with no effect on mitochondrial ROS (Figures 2D, E2D-E) or activated Cathepsin B production (Figures 2E-F). Calcineurin-dependent effects on phagosomal maturation were analysed by phagosomal acidification and recruitment of the late phagosomal maturation marker, LAMP-1 to *Af*-containing phagosomes. Calcineurin inhibition increased LAMP-1 recruitment at early time points after infection ( $P<0.05$ ) (Figure E2F, E2G). Phagosomal acidification was not calcineurin-dependent (Figures E2H, E2I). These results indicate that inhibition of the calcineurin-NFAT pathway impairs the ability of human macrophages to control fungal hyphal transition, delays fungal phagocytosis, and reduces ROS production.

### **Macrophages traffic *Af*-containing endosomes to neighbouring cells through calcineurin-dependent lateral transfer**

During live time-lapse confocal imaging, we observed lateral transfer of germinating *Af* between hMDMs (Figure 3A, Movie 1). This was confirmed in alveolar macrophages from lung transplant recipients (Movie 2). Lateral transfer events occurred in  $3.0 \pm 0.4\%$  of cells infected with SC, peaking at 4 to 6 h p.i. (Figure 3B). Calcineurin inhibition markedly reduced lateral transfer ( $53.9\% \pm 10.3$ ) ( $P=0.002$ ) (Figure 3C).

We assessed the role of fungal germination in lateral transfer of *Af* by time-lapse microscopy of metabolically inactive RC or dead fixed SC. Lateral transfer was dependent on both live and swollen *Af* ( $P<0.001$ ) (Figure 3D). We observed co-localisation of actin and

dynamins to conidia undergoing lateral transfer (Figures 3E,3F) suggesting an actin and dynamin-dependent process. This was confirmed by treating hMDMs with actin polymerisation or dynamin inhibitors (Cytochalasin D or Dynasore respectively) following phagocytosis ( $P<0.001$ ) (Figure 3D). Fungal burden was increased after inhibition of lateral transfer post-phagocytosis using Dynasore, suggesting transfer enables recipient macrophage control of hyphal germination ( $P<0.01$ ) (Figure E3A). Transmission electron microscopy showed that transfer of *Af*-containing cargo between hMDMs occurred in membrane-bound compartments (Figure E3B). The *Af*-containing cargo transferred between hMDMs was further characterized by staining for endo-lysosomal markers (Rab 5, Rab7 and LAMP-1). This showed that *Af* was transferred between hMDMs in Rab7-positive and Rab5 and LAMP-1-negative compartments, suggesting late endosomal trafficking (Figure 3F and E3C).

To determine whether this phenomenon occurred *in vivo*, we exploited our zebrafish invasive aspergillosis model (4). Using an mpeg:mCherry transgenic zebrafish line and eGFP-expressing *Af*, we examined the macrophage-*Af* interaction *in vivo* using time-lapse high-resolution confocal microscopy. We observed similar macrophage *Af* lateral transfer in zebrafish larvae, consistent with an evolutionarily conserved macrophage response to *Af* infection that occurs *in vivo* (Figure 3G and Movie 3). Taken together, these observations indicate that successful fungal germination in the late endosome triggers exocytic transfer of *Af* between macrophages.

**Macrophages undergoing calcineurin-dependent programmed necrosis transfer *Af* conidia to neighbouring cells to control fungal germination**

hMDMs transferring *Af* had increasingly translucent cytoplasm, organelle swelling and increased cell volume, suggesting programmed cell death during transfer. This was confirmed by confocal microscopy using propidium iodide (PI) (Figure 4A, Movie 4). Around 90% of macrophages successfully control fungal germination and do not die (Figure 4B). PI staining revealed that in dying macrophages ( $13 \pm 2\%$ ), lateral transfer occurred in  $37 \pm 5\%$  (Figure 4D). This represents  $\sim 3\text{-}4\%$  of total macrophages as previously described infected with *Af* SC. Transfer of *Af* conidia from dying hMDMs enhanced control of germination, compared to dying hMDMs where conidia were not transferred ( $P=0.003$ ) (Figure 4B). Germination of *Af* in live hMDMs was well controlled when compared to cells undergoing programmed necrosis (Figure E3D), further supporting a model where programmed cell death and lateral transfer occur in response to successful fungal germination in macrophages, to enable containment of infection in recipient macrophages (Figure 4B).

Consistent with programmed cell death, we observed massive vacuole formation adjacent to the *Af*-containing compartment (Figure E3E, Movie 5) (24). Transmission electron microscopy also showed conidia residing within large vacuoles (Figure E3F). Vacuole formation was inhibited by pre-treatment with the vacuolar H<sup>+</sup> ATPase inhibitor Bafilomycin ( $P=0.003$ ), with a trend towards decreased transfer ( $P=0.06$ ) (Figure E3G).

To define the relationship between cell death and transfer, induction of necroptosis with the pan-caspase inhibitor Z-VAD-FMK (an inhibitor of caspase-dependent apoptosis which increases necroptosis) was performed (25, 26). This increased lateral transfer ( $P=0.003$ ) (Figure 4C). Addition of Necrostatin-1, an inhibitor of RIP1 kinase-dependent necroptosis, to Z-VAD-FMK, inhibited both cell death ( $P=0.078$ ) and lateral transfer ( $P=0.028$ ) induced by Z-VAD-FMK alone (Figure 4C). However, induction of necroptosis with Z-VAD-FMK led to

increased fungal burden due to recipient macrophage death ( $P<0.01$ ) (Figure E3H). Necrostatin-1 alone or necrosulphonamide could not inhibit macrophage programmed cell death or lateral transfer (Figure 4C). As pyroptosis has recently been shown following macrophage infection with *C. albicans*, we blocked pyroptosis with an irreversible cell permeable caspase-1 inhibitor, (Z-YVAD-FMK), which did not affect cell death or lateral transfer (Figure 4C) (27). These observations are consistent with transfer of *Af* between macrophages during a programmed cell death process with hallmarks of necroptosis.

As calcineurin regulates cell death, we assessed its role in macrophage necrosis following infection (28). Calcineurin inhibition reduced macrophage programmed necrosis by 57% +/- 13.7 ( $P=0.01$ ) (Figure 4D) and was associated with accelerated fungal germination at late time-points in macrophages that failed to undergo necrosis-dependent transfer ( $P<0.001$ ) (Figures E3I, E3J). This is consistent with a calcineurin-dependent checkpoint for programmed necrosis during *Af* germination.

Together, these results indicate that hMDMs infected with live *Af* SC undergo calcineurin-dependent cell death with hallmarks of programmed necroptosis and transfer *Af*-containing endosomes to neighbouring cells to facilitate control of fungal germination.

### **Calcineurin regulates cell death and the MAP kinase pathway during *Af* infection**

To further define the macrophage response to *Af*, we undertook next generation transcript profiling of hMDMs during phagocytosis. hMDMs pre-treated with FK506 were infected with SC for 1h or 6h, and differentially expressed genes compared to baseline and untreated infection controls were identified (Figure E4A). The major gene sets regulated by calcineurin at 6h p.i. were associated with cell death, inflammatory responses and transcriptional

regulation (Figure E4B). 51 genes associated with the cell death pathway were calcineurin-dependent at 6h p.i (Table E1).

Over-representation analysis using ConsensusPathDB (CPDB) identified calcineurin-dependent control of the programmed cell death, MAPK signalling and cytokine-cytokine interaction pathways at 6h p.i. (Figure E4C). To assess the interaction between the pathways regulated by calcineurin, a protein-protein interactions (PPI) network was created. This identified significant interactions and clustering of transcriptional regulation pathways, immune response pathways, apoptosis and the AP-1 transcription factor network (Figure 4E). Studies have suggested a critical role for the MAPK-AP-1 pathway, and dynamin-related protein 1(Drp1)-mediated mitochondrial fission in necroptosis (25, 29). As mitochondrial translocation of Drp1 and MAPK-AP-1 pathway regulation are thought to be calcineurin-dependent, this was explored in *Af*-infected hMDMs (30-32). Significant modulation of MAPK-AP-1 pathway activation and Ser637 P-Drp1 phosphorylation was observed (Figure E4D). Thus, RNA- and protein-level analyses further support a role for calcineurin in the macrophage programmed cell death response to *Af*.

#### ***Af* containing endosomes transferred from macrophages to macrophage are enveloped within actin-VASP rich cargo**

Calcineurin phosphatase activity has multiple NFAT-independent effects on cytoskeletal reorganisation and regulation of MAPK pathways (31, 33, 34). To identify calcineurin phosphatase targets, we performed a comparative phosphoproteomic array on FK506 vs. vehicle pre-treated hMDMs infected with SC (Figure 5A). There were differences in phosphorylation of proteins within the MAPK pathway including c-Jun, and the cell cycle

regulatory protein CDC25A. This is consistent with our transcriptomic findings of cross-control between calcineurin, and MAPK pathways and cell death pathways.

The analysis revealed a 26-fold increase in Ser238 phosphorylated vasodilator-stimulated phosphoprotein (VASP) levels in FK506-treated hMDMs (Figure 5A). VASP is an actin polymerase that promotes assembly of actin networks, and is important for directional motility and phagocytosis (35-37). Its function is tightly regulated with Ser238 dephosphorylation required for actin filament formation. We therefore postulated that VASP is a direct calcineurin target. As calcineurin is the only  $\text{Ca}^{2+}$ -activated serine-threonine phosphatase, we measured Ser238 P-VASP following the addition of the calcium ionophore ionomycin (to selectively activate calcineurin) to hMDMs with phosphorylated VASP (induced using a cell permeable cGMP analogue) in the presence or absence of FK506 (Figure 5B). This confirmed that VASP is a major dephosphorylation target of calcineurin.

As VASP is an important actin cytoskeletal regulator, and calcineurin is required for optimal phagocytosis and transfer of *Af*, we hypothesized that VASP is involved in actin-dependent phagocytosis and lateral transfer of *Af*. Using high-resolution confocal microscopy, we observed co-localisation of VASP to *Af* at phagocytic cups, which disappeared following internalisation (Figures 5C, 5D and Movie 6). Localisation of VASP to *Af* was not calcineurin-dependent. During *Af* lateral transfer at late time-points, high intensity co-localisation of VASP and actin staining was observed to *Af*-containing endosomes (Figure 5E). High-resolution 3D reconstruction revealed that *Af* containing endosomes trafficked between macrophages are enveloped within actin-VASP rich cargo (Figure 5C-G and Movie 7).

To determine the role of VASP in macrophage *Af* phagocytosis, siRNA knockdown of VASP was performed in human macrophages, followed by analysis of uptake of calcofluor white-

stained live *Af* SC compared to control. This showed that phagocytosis of live *Af* SC at early time-points is VASP-dependent ( $P < 0.01$ ) (Figure 5H), consistent with the defect seen for calcineurin inhibition (Figure 2B). Taken together, these results indicate that calcineurin has a key role in macrophage actin cytoskeleton re-organisation during fungal infection, by direct de-phosphorylation and activation of the actin polymerase VASP. This enables optimal actin-dependent *Af* phagocytosis and lateral transfer of *Af* containing endosomes during programmed necrosis, which are critical to achieve control of germinating conidia.

## Discussion

Pulmonary aspergillosis has emerged as a serious infectious complication of a range of immunocompromised states and chronic respiratory diseases. Overt infection is typically characterised by hyper-inflammatory tissue destruction, with more complex relationships between airway colonization and progression of chronic respiratory diseases (38). Here we report human macrophage programmed necrosis as an important response to germination of *Af*. Whilst necrosis has been recognized as a form of cell death since the mid-nineteenth century, it has recently become clear that programmed necrosis may occur through receptor-interacting protein kinase 3 (RIPK3) necroptotic cell death (39). Necroptosis occurs as a first line defense to intracellular pathogens, and is central to the pathogenesis of a number of chronic inflammatory conditions including emphysematous change (40, 41).

Remarkably, we observed frequent lateral transfer of *Af* during necroptosis which ultimately enabled control of hyphal escape from the macrophage. Transfer occurred through a late endosomal compartment, suggesting that this process may have similarities to exocytosis (42). Whilst lateral transfer has previously been observed for *Cryptococcus neoformans* at

low frequency, the molecular basis for transfer and its relationship to cell death or control of infection have not been previously defined (43). The pathogen escape and transfer processes described to date are pathogen-mediated, and enhance either tissue dissemination, or evasion from immune attack (47). However, our observations are consistent with host-dependent lateral transfer of *Af*, to limit hyphal escape during macrophage death. The observation of cell-cell transfer of *Af* supports a model whereby inhaled conidia may persist in the myeloid compartment as spores for prolonged periods of time. This has potentially important implications for individuals who subsequently undergo immunosuppression.

Notably, we observed that both fungal-driven programmed necrosis and lateral transfer were calcineurin-dependent, indicating that necroptotic control of infection is likely to be impaired in organ transplantation. Calcineurin has been postulated to have a role in the regulation of programmed cell death through interaction with Bcl-2 family proteins (25, 26). Consistent with this, we found significant calcineurin-dependent expression of Myeloid Cell Leukaemia 1 (MCL1), a Bcl-2 protein that inhibits apoptosis, and Bcl2 Modifying Factor (BMF), a member of the pro-death BH3-only subgroup of Bcl-2 family proteins required for TNF $\alpha$ -induced necroptosis (27). Transcriptomic and phosphoproteomic analysis defined calcineurin as a key phosphatase mediating cross-control of cell death, the MAPK-AP-1 innate pathway, and VASP-dependent cytoskeletal remodelling during macrophage infection. Calcineurin inhibition impaired these cellular processes, leading to enhanced fungal germination in the late phagosome, impaired lateral transfer, and ultimately hyphal escape. Interestingly, virulent *Burkholderia spp.* have recently been shown to mimic VASP

actin polymerases to enable cell fusion and spread (44). Whether fungi are able to directly manipulate host actin polymerases remains to be determined.

In summary, we have identified macrophage programmed necrosis as an important response to progressive germination of *Aspergillus fumigatus* in the human macrophage, and report a previously undescribed phenomenon of cell death-dependent lateral transfer as a co-operative macrophage behaviour that assists in limiting hyphal escape. We show that calcineurin is a key orchestrator of this process, further defining the importance of this pathway in innate immunity. Our findings yield novel insights into host innate immunity to *Af* in the lung, extend current understanding of the pathogenesis of PA in organ transplantation, and have broader implications for transplant immunity and chronic lung disease.

### **Acknowledgements**

We thank the patients of the Royal Brompton and Harefield Hospitals UK who participated in this study. This project was supported by the NIHR Respiratory Disease Biomedical Research Unit and the Imperial College Academic Health Science Centre. We thank Avinash Shenoy and Jason Mercer for helpful discussions and the Imperial Facility for Imaging and Light Microscopy and Amelia Shoemark for technical support.

### **REFERENCES**

1. Latge JP. *Aspergillus fumigatus* and aspergillosis. *Clinical microbiology reviews* 1999;12:310-350.

2. Bhatia S, Fei M, Yarlagadda M, Qi Z, Akira S, Saijo S, Iwakura Y, van Rooijen N, Gibson GA, St Croix CM, Ray A, Ray P. Rapid host defense against aspergillus fumigatus involves alveolar macrophages with a predominance of alternatively activated phenotype. *PLoS one* 2011;6:e15943.
3. Chen GH, Teitz-Tennenbaum S, Neal LM, Murdock BJ, Malachowski AN, Dils AJ, Olszewski MA, Osterholzer JJ. Local gm-csf-dependent differentiation and activation of pulmonary dendritic cells and macrophages protect against progressive cryptococcal lung infection in mice. *Journal of immunology* 2016;196:1810-1821.
4. Herbst S, Shah A, Mazon Moya M, Marzola V, Jensen B, Reed A, Birrell MA, Saijo S, Mostowy S, Shaunak S, Armstrong-James D. Phagocytosis-dependent activation of a tlr9-btk-calcineurin-nfat pathway co-ordinates innate immunity to aspergillus fumigatus. *EMBO molecular medicine* 2015;7:240-258.
5. Herbst S, Shah A, Carby M, Chusney G, Kikkeri N, Dorling A, Bignell E, Shaunak S, Armstrong-James D. A new and clinically relevant murine model of solid-organ transplant aspergillosis. *Disease models & mechanisms* 2013;6:643-651.
6. Espinosa V, Jhingran A, Dutta O, Kasahara S, Donnelly R, Du P, Rosenfeld J, Leiner I, Chen CC, Ron Y, Hohl TM, Rivera A. Inflammatory monocytes orchestrate innate antifungal immunity in the lung. *PLoS pathogens* 2014;10:e1003940.
7. Kosmidis C, Denning DW. The clinical spectrum of pulmonary aspergillosis. *Thorax* 2015;70:270-277.
8. Pappas PG, Alexander BD, Andes DR, Hadley S, Kauffman CA, Freifeld A, Anaissie EJ, Brumble LM, Herwaldt L, Ito J, Kontoyiannis DP, Lyon GM, Marr KA, Morrison VA, Park BJ, Patterson TF, Perl TM, Oster RA, Schuster MG, Walker R, Walsh TJ, Wannemuehler KA, Chiller TM. Invasive fungal infections among organ transplant recipients: Results of the transplant-associated infection surveillance network (transnet). *Clinical infectious diseases : an official publication of the Infectious Diseases Society of America* 2010;50:1101-1111.
9. Armstrong-James D, Teo I, Herbst S, Petrou M, Shiu KY, McLean A, Taube D, Dorling A, Shaunak S. Renal allograft recipients fail to increase interferon-gamma during invasive fungal diseases. *American journal of transplantation : official journal of the American Society of Transplantation and the American Society of Transplant Surgeons* 2012;12:3437-3440.
10. Hogan C, Denning DW. Allergic bronchopulmonary aspergillosis and related allergic syndromes. *Seminars in respiratory and critical care medicine* 2011;32:682-692.
11. Denning DW, Pleuvry A, Cole DC. Global burden of allergic bronchopulmonary aspergillosis with asthma and its complication chronic pulmonary aspergillosis in adults. *Medical mycology : official publication of the International Society for Human and Animal Mycology* 2013;51:361-370.
12. Ader F, Nseir S, Le Berre R, Leroy S, Tillie-Leblond I, Marquette CH, Durocher A. Invasive pulmonary aspergillosis in chronic obstructive pulmonary disease: An emerging fungal pathogen. *Clin Microbiol Infect* 2005;11:427-429.
13. Maturu VN, Agarwal R. Prevalence of aspergillus sensitization and allergic bronchopulmonary aspergillosis in cystic fibrosis: Systematic review and meta-analysis. *Clinical and experimental allergy : journal of the British Society for Allergy and Clinical Immunology* 2015.

14. Taccone FS, Van den Abeele AM, Bulpa P, Misset B, Meersseman W, Cardoso T, Paiva JA, Blasco-Navalpotro M, De Laere E, Dimopoulos G, Rello J, Vogelaers D, Blot SI, Asp ICUSI. Epidemiology of invasive aspergillosis in critically ill patients: Clinical presentation, underlying conditions, and outcomes. *Critical care* 2015;19:7.
15. Taylor AL, Watson CJ, Bradley JA. Immunosuppressive agents in solid organ transplantation: Mechanisms of action and therapeutic efficacy. *Critical reviews in oncology/hematology* 2005;56:23-46.
16. Goodridge HS, Simmons RM, Underhill DM. Dectin-1 stimulation by candida albicans yeast or zymosan triggers nfat activation in macrophages and dendritic cells. *Journal of immunology* 2007;178:3107-3115.
17. Tourneur E, Ben Mkaddem S, Chassin C, Bens M, Goujon JM, Charles N, Pellefigues C, Aloulou M, Hertig A, Monteiro RC, Girardin SE, Philpott DJ, Rondeau E, Elbim C, Werts C, Vandewalle A. Cyclosporine a impairs nucleotide binding oligomerization domain (nod1)-mediated innate antibacterial renal defenses in mice and human transplant recipients. *PLoS pathogens* 2013;9:e1003152.
18. Kim D, Pertea G, Trapnell C, Pimentel H, Kelley R, Salzberg SL. Tophat2: Accurate alignment of transcriptomes in the presence of insertions, deletions and gene fusions. *Genome biology* 2013;14:R36.
19. Trapnell C, Roberts A, Goff L, Pertea G, Kim D, Kelley DR, Pimentel H, Salzberg SL, Rinn JL, Pachter L. Differential gene and transcript expression analysis of rna-seq experiments with tophat and cufflinks. *Nature protocols* 2012;7:562-578.
20. Dennis G, Jr., Sherman BT, Hosack DA, Yang J, Gao W, Lane HC, Lempicki RA. David: Database for annotation, visualization, and integrated discovery. *Genome biology* 2003;4:P3.
21. Bader GD, Hogue CW. An automated method for finding molecular complexes in large protein interaction networks. *BMC bioinformatics* 2003;4:2.
22. Philippe B, Ibrahim-Granet O, Prevost MC, Gougerot-Pocidallo MA, Sanchez Perez M, Van der Meeren A, Latge JP. Killing of aspergillus fumigatus by alveolar macrophages is mediated by reactive oxidant intermediates. *Infection and immunity* 2003;71:3034-3042.
23. Mittal A, Gahlaut A, Sharma GL, Dabur R. Antifungal treatments delineate a correlation between cathepsins and cytokines in murine model of invasive aspergillosis. *Indian journal of pharmaceutical sciences* 2013;75:688-699.
24. Chan FKM. Fueling the flames: Mammalian programmed necrosis in inflammatory diseases. *Csh Perspect Biol* 2012;4.
25. Wu YT, Tan HL, Huang Q, Sun XJ, Zhu X, Shen HM. Zvad-induced necroptosis in I929 cells depends on autocrine production of tnfa mediated by the pkc-mapks-ap-1 pathway. *Cell death and differentiation* 2011;18:26-37.
26. Kim SJ, Li J. Caspase blockade induces rip3-mediated programmed necrosis in toll-like receptor-activated microglia. *Cell death & disease* 2013;4:e716.

27. Krysan DJ, Sutterwala FS, Wellington M. Catching fire: *Candida albicans*, macrophages, and pyroptosis. *PLoS pathogens* 2014;10:e1004139.
28. Erin N, Bronson SK, Billingsley ML. Calcium-dependent interaction of calcineurin with bcl-2 in neuronal tissue. *Neuroscience* 2003;117:541-555.
29. Kanamaru Y, Sekine S, Ichijo H, Takeda K. The phosphorylation-dependent regulation of mitochondrial proteins in stress responses. *Journal of signal transduction* 2012;2012:931215.
30. Cereghetti GM, Stangherlin A, Martins de Brito O, Chang CR, Blackstone C, Bernardi P, Scorrano L. Dephosphorylation by calcineurin regulates translocation of drp1 to mitochondria. *Proceedings of the National Academy of Sciences of the United States of America* 2008;105:15803-15808.
31. Huang CC, Wang JM, Kikkawa U, Mukai H, Shen MR, Morita I, Chen BK, Chang WC. Calcineurin-mediated dephosphorylation of c-jun ser-243 is required for c-jun protein stability and cell transformation. *Oncogene* 2008;27:2422-2429.
32. Wu CC, Hsu SC, Shih HM, Lai MZ. Nuclear factor of activated t cells c is a target of p38 mitogen-activated protein kinase in t cells. *Molecular and cellular biology* 2003;23:6442-6454.
33. Zhao JW, Gao ZL, Ji QY, Wang H, Zhang HY, Yang YD, Xing FJ, Meng LJ, Wang Y. Regulation of cofilin activity by camkii and calcineurin. *The American journal of the medical sciences* 2012;344:462-472.
34. Escolano A, Martinez-Martinez S, Alfranca A, Urso K, Izquierdo HM, Delgado M, Martin F, Sabio G, Sancho D, Gomez-del Arco P, Redondo JM. Specific calcineurin targeting in macrophages confers resistance to inflammation via mcp-1 and p38. *The EMBO journal* 2014;33:1117-1133.
35. Hansen SD, Mullins RD. Vasp is a processive actin polymerase that requires monomeric actin for barbed end association. *Journal of Cell Biology* 2010;191:571-584.
36. Krause M, Dent EW, Bear JE, Loureiro JJ, Gertler FB. Ena/vasp proteins: Regulators of the actin cytoskeleton and cell migration. *Annual review of cell and developmental biology* 2003;19:541-564.
37. Coppolino MG, Krause M, Hagendorff P, Monner DA, Trimble W, Grinstein S, Wehland J, Sechi AS. Evidence for a molecular complex consisting of fyb/slap, slp-76, nck, vasp and wasp that links the actin cytoskeleton to fcgamma receptor signalling during phagocytosis. *Journal of cell science* 2001;114:4307-4318.
38. Warris A. The biology of pulmonary aspergillus infections. *The Journal of infection* 2014;69 Suppl 1:S36-41.
39. Linkermann A, Green DR. Necroptosis. *The New England journal of medicine* 2014;370:455-465.
40. Silke J, Rickard JA, Gerlic M. The diverse role of rip kinases in necroptosis and inflammation. *Nature immunology* 2015;16:689-697.

41. Mizumura K, Cloonan SM, Nakahira K, Bhashyam AR, Cervo M, Kitada T, Glass K, Owen CA, Mahmood A, Washko GR, Hashimoto S, Ryter SW, Choi AM. Mitophagy-dependent necroptosis contributes to the pathogenesis of copd. *The Journal of clinical investigation* 2014;124:3987-4003.
42. Szumowski SC, Estes KA, Popovich JJ, Botts MR, Sek G, Troemel ER. Small gtpases promote actin coat formation on microsporidian pathogens traversing the apical membrane of caenorhabditis elegans intestinal cells. *Cellular microbiology* 2016;18:30-45.
43. Johnston SA, May RC. The human fungal pathogen cryptococcus neoformans escapes macrophages by a phagosome emptying mechanism that is inhibited by arp2/3 complex-mediated actin polymerisation. *PLoS pathogens* 2010;6:e1001041.
44. Benanti EL, Nguyen CM, Welch MD. Virulent burkholderia species mimic host actin polymerases to drive actin-based motility. *Cell* 2015;161:348-360.

## Figure Legends

### **Figure 1. *A. fumigatus* activates calcineurin-NFAT-dependent inflammatory responses in human macrophages**

(A) hMDMs were stimulated with live *Af* SC (MOI=1). hMDM nuclear extracts were collected at 30, 60 and 120min p.i. and probed by Western blot for NFATc2. Maximum translocation of NFATc2 to the nucleus was observed at 60 minutes p.i. Western shown representative of data from n= 4.

(B-C) hMDMs were pre-treated with FK506 (10ng/ml) and stimulated with live *Af* SC (MOI=1). Nuclear extracts were probed by western blot for NFACTc2 and whole cell extracts for RCAN1. NFAT translocation was assessed by confocal microscopy. NFAT shown in red, nuclei in blue and *Af* conidia are seen in green. Representative images are shown of live conidia stimulating NFAT nuclear translocation. Western shown representative of data from n= 4.

(D) hMDMs were pre-treated with FK506 (10ng/ml) and stimulated with live *Af* SC (MOI=1). FK506 completely inhibited RCAN1 production. Western shown representative of data from n= 4.

(E) hMDMs were pre-treated with FK506 (10ng/ml) and stimulated with live *Af* SC (MOI=1). Culture supernatant cytokines were measured at 6hr p.i. by Luminex. N =7

### **Figure 2. Human macrophage phagocytosis, reactive oxygen species production and control of *A. fumigatus* growth are calcineurin dependent**

(A) hMDMs pre-treated with FK506 (10ng/ml) or vehicle were stimulated with live *Af* SC (MOI=1), and total RNA isolated at 1 and 6 hour p.i. Fungal growth was assayed by RT-PCR of fungal RNA. N = 5

(B) hMDMs pre-treated with FK506 (10ng/ml) or vehicle were infected with live eGFP-expressing *Af* SC (MOI=1), and hyphal transition assessed using time-lapse video microscopy over a 10h period. N = 4

(C) hMDMs pre-treated with FK506 (10ng/ml) or cytochalasin D (5nM) or vehicle were stimulated with live *Af* SC (MOI=1) prestained with Calcofluor white. Phagocytosis was quantified by Imagestream. p.i. N=4

(D) hMDMs pre-treated with FK506 (10ng/ml) or vehicle were stimulated with live *Af* SC (MOI=1) and ROS production assayed by luminescence. N=4

(E) hMDMs pre-treated with FK506 (10ng/ml) or vehicle were stimulated with live *Af* SC (MOI=1) and Cathepsin B activation assayed by live confocal time-lapse microscopy. Phagosomal activated Cathepsin B activation was quantified by *ImageJ*. N=4

(F) Representative confocal microscopy image showing Cathepsin B activation in *Af* conidia containing phagosomes in MDMs. Activated Cathepsin B is shown in red, nuclei in blue and *Af* in green. Data are represented as mean  $\pm$  SEM.

**Figure 3. Macrophages infected with swollen *A. fumigatus* undergo calcineurin-dependent lateral transfer.**

(A) Representative time-lapse widefield microscopy images of *Af* lateral transfer in MDMs infected with live *Af* SC (MOI=1, shown in green). Transferring macrophage labelled 'a' and receiving macrophage labelled 'b'. Images taken at 10 minute intervals.

(B) hMDMs were stimulated with live eGFP-*Af* SC (MOI=1) and time-lapse widefield imaging performed at 10min intervals for 12h p.i.. Timing of lateral transfer events per hour in macrophages infected with live *Af* SC is shown (N=3).

(C) hMDMs pre-treated with FK506 (10ng/ml) or vehicle were stimulated with live eGFP-*Af* SC (MOI=1) and lateral transfer events quantified by time-lapse widefield imaging at 10 minute intervals for 12 hour p.i. (N=5). Total lateral transfer events over the 12h period were quantified for each biological replicate.

(D) hMDMs were stimulated with live or fixed *Af* SC or RC (MOI=1) and lateral transfer events quantified by time-lapse widefield microscopy. Cytochalasin D (5nM) and Dynasore (100µM) were added at 90mins p.i. with unbound conidia washed away 45mins p.i.. N=4

(E) Representative confocal microscopy image of dynamin-dependent lateral transfer in monocyte-derived macrophages stimulated with live *Af* SC. Dynamin shown in red, nuclei in blue and *Af* in green.

(F) MDMs were stimulated with live *Af* SC (MOI=1) with non-phagocytosed conidia washed away at 45mins p.i.. Lateral transfer events were captured by fixing cells every 10mins from 120-180mins p.i.. Characterisation of *Af* lateral transfer was performed by staining for Rab 5, Rab 7 and LAMP-1 (shown in red) alongside actin (shown in cyan). Nuclei are shown in blue and live swollen *Af* in green. Representative images show positive Rab7 localisation to *Af*

containing endosomes during lateral transfer with little Rab 5 localisation and no LAMP-1 localisation.

(G) MPEG:mCherry Zebrafish larvae were infected with ~50 eGFP-expressing conidia of *Af* and time-lapse confocal microscopy performed. Representative images show *Af* lateral transfer between macrophages. The transferring macrophage is labelled 'a' and the receiving macrophage labelled 'b'. Images shown are at 7 minute intervals. Data are represented as mean  $\pm$  SEM.

**Figure 4. Macrophages undergoing programmed necrosis laterally transfer germinating *A. fumigatus* conidia in endosomes through an actin-dependent process.**

(A) Representative time-lapse confocal microscopy images of lateral transfer of live *Af* SC (shown in green) between MDMs. Propidium iodide staining (red) showing cell death of macrophage transferring *Af* conidia (labelled 'a') to neighbouring macrophage (labelled 'b'). Images taken at 10 minute intervals.

(B) Time-lapse confocal microscopy was used to quantify the fate of transferred vs non-transferred conidia from dying human MDMs and to conidia within live macrophages. Germination was assessed over a 12-hour period. Control of fungal germination was significantly increased in dying hMDMs that transferred conidia to neighbouring cells compared to those that did not. N=4

(C) hMDMs pre-treated with a pan-caspase inhibitor (Z-VAD-FMK 50 $\mu$ M), RIPK-1 inhibitor (Necrostatin-1 10 $\mu$ M), caspase-1 inhibitor (Z-YVAD-FMK 50 $\mu$ M), FK506 10ng/ml or vehicle were stimulated with live *Af* SC (MOI=1) and lateral transfer events and cell death quantified by propidium iodide fluorescence based time-lapse confocal microscopy. Treatment with Z-

VAD-FMK induced necroptotic cell death coupled to increased *Af* lateral transfer, which was inhibited by the addition of a RIPK-1 inhibitor (Necrostatin-1). N=3

(D) hMDMs pre-treated FK506 (10ng/ml) or vehicle were stimulated with live *Af* SC (MOI=1) and cell death assayed by propidium iodide fluorescence quantified by time-lapse confocal microscopy over a 6h period. The graph also shows the proportion of lateral transfer events in dying cells (~30% of dying cells). N=4

(E) The network modules of the significantly expressed genes in FK506 pre-treated macrophages stimulated with live *Af* SC (MOI=1) for 6hrs. Significantly expressed genes were mapped on to PPI network and network modules identified using the MCODE plugin application of Cytoscape. Over represented pathway involving these network modules were identified from the KEGG and Wikipathways databases. N=6. Data are represented as mean  $\pm$  SEM.

**Figure 5. Lateral transfer of *Aspergillus fumigatus* occurs through VASP tunnel-like structures.**

(A) A phosphoprotein array analysis of hMDMs pre-treated with FK506 and stimulated with live *Af* SC (MOI=1) for 1hr p.i was performed. Proteins with significant fold change differences in the phosphoprotein to non-phosphoprotein ratio between FK506 and control macrophages stimulated with live *Af* SC are shown.

(B) hMDMs were pre-treated with a cell-permeable cGMP analogue (8-pCPT-cGMP 25mM) to induce Ser238 VASP phosphorylation and FK506 (10ng/ml) or vehicle. They were then stimulated with a calcium ionophore (Ionomycin 2 $\mu$ g/ml) to activate calcineurin.

Macrophage whole cell extracts were probed by western blot for Ser238 VASP and total VASP.

(C) Representative confocal microscopy images of hMDM phagocytosis and lateral transfer of live *Af* SC (MOI=1). VASP shown in red, nuclei in blue and *Af* in green. 1: Uninfected hMDMs; 2: Initial phagocytosis of *Af* by MDMs; 3: Late phagocytosis of *Af* by hMDMs; 4: Lateral transfer of *Af* between hMDMs.

(D) 3D reconstruction of confocal microscopy images of phagocytosis and lateral transfer of live *Af* SC (MOI=1) between hMDMs. Image of *Af* phagocytosis at 30min p.i. with VASP shown in red, *Af* in green and nuclei in blue.

(E) 3D reconstruction of confocal microscopy image of *Af* lateral transfer with VASP shown in yellow, actin in magenta, *Af* in green and nuclei in blue.

(F-G) Representative z-slice confocal microscopy image (F) and 3D reconstruction (G) of *Af* lateral transfer. VASP shown in red, *Af* in green.

(H) THP-1 macrophages treated with either control or VASP siRNA (50 $\mu$ M) were infected with live *Af* SC and stained with calcofluor-white (Sigma) (MOI=1). Phagocytosis was quantified by flow cytometry. N=3. Data are represented as mean  $\pm$  SEM.

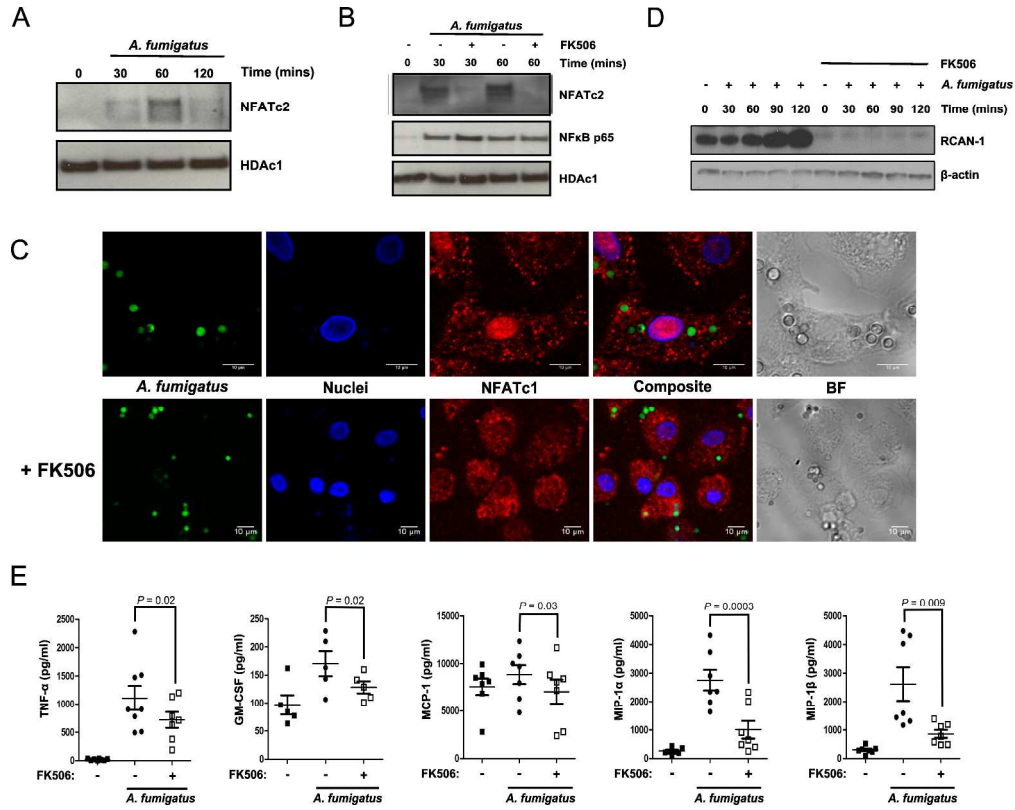


Figure 1. *A. fumigatus* activates calcineurin-NFAT-dependent inflammatory responses in human macrophages

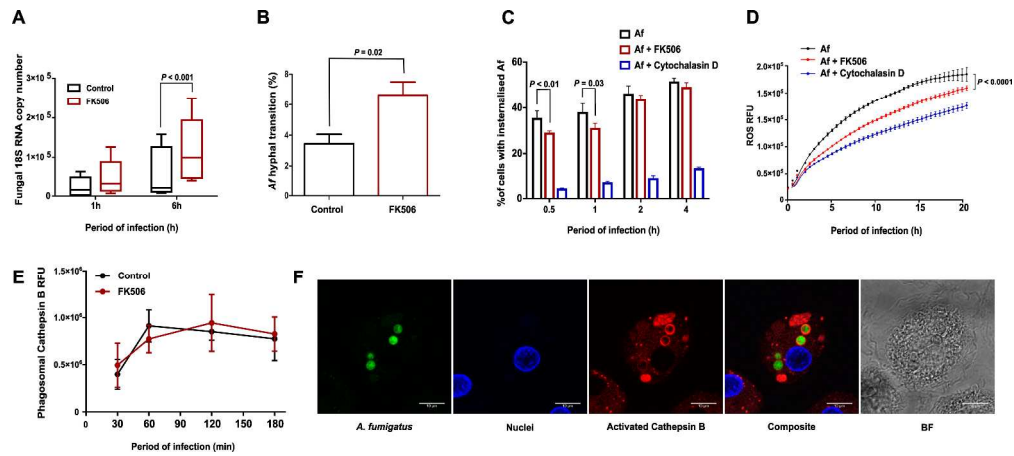
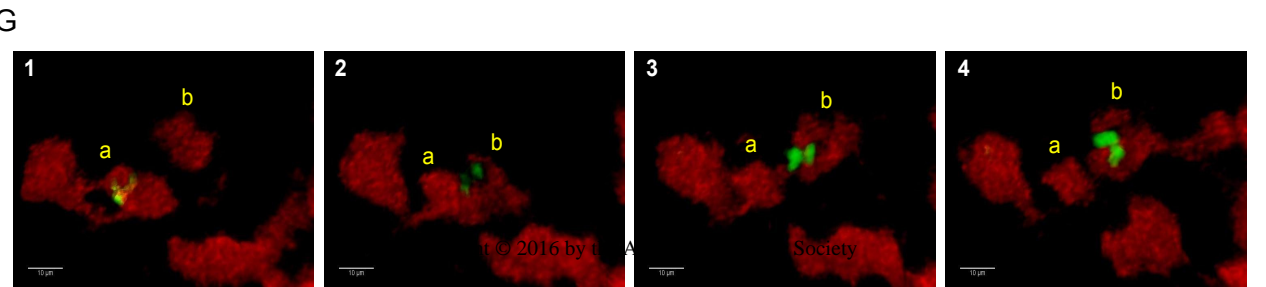
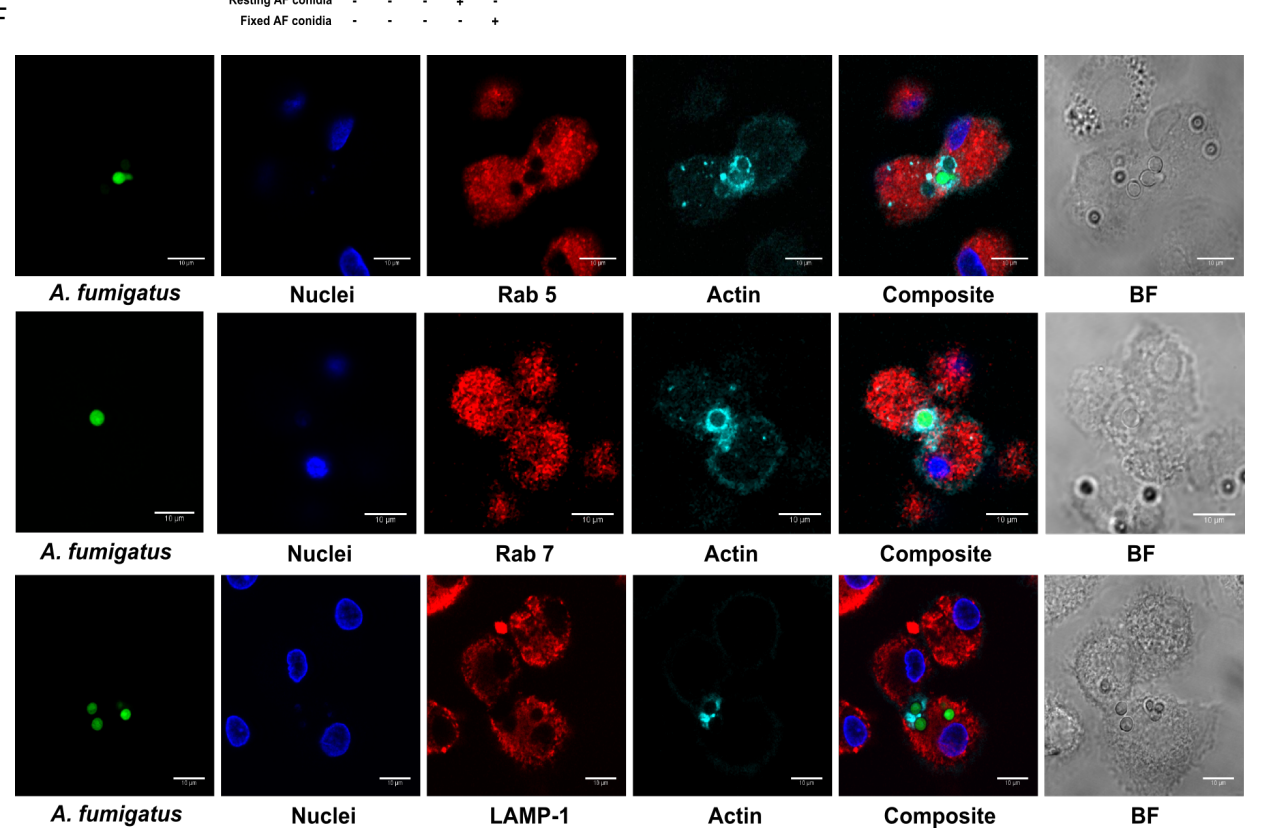
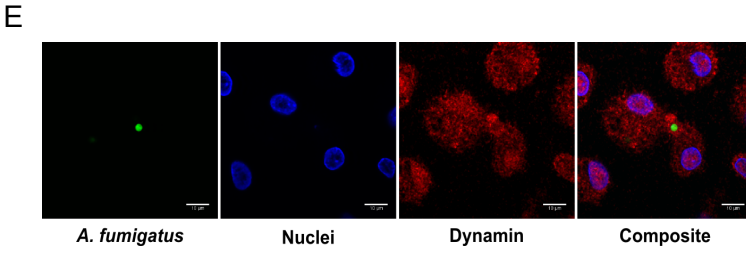
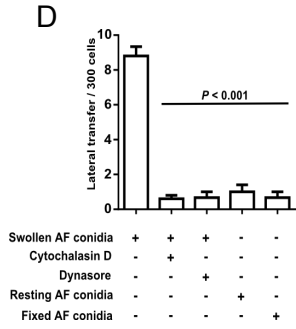
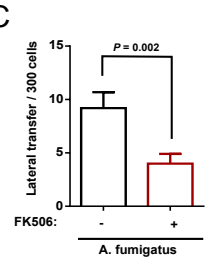
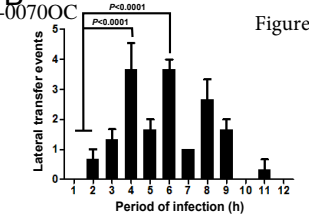
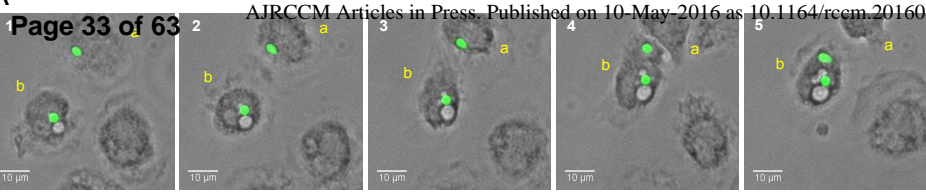
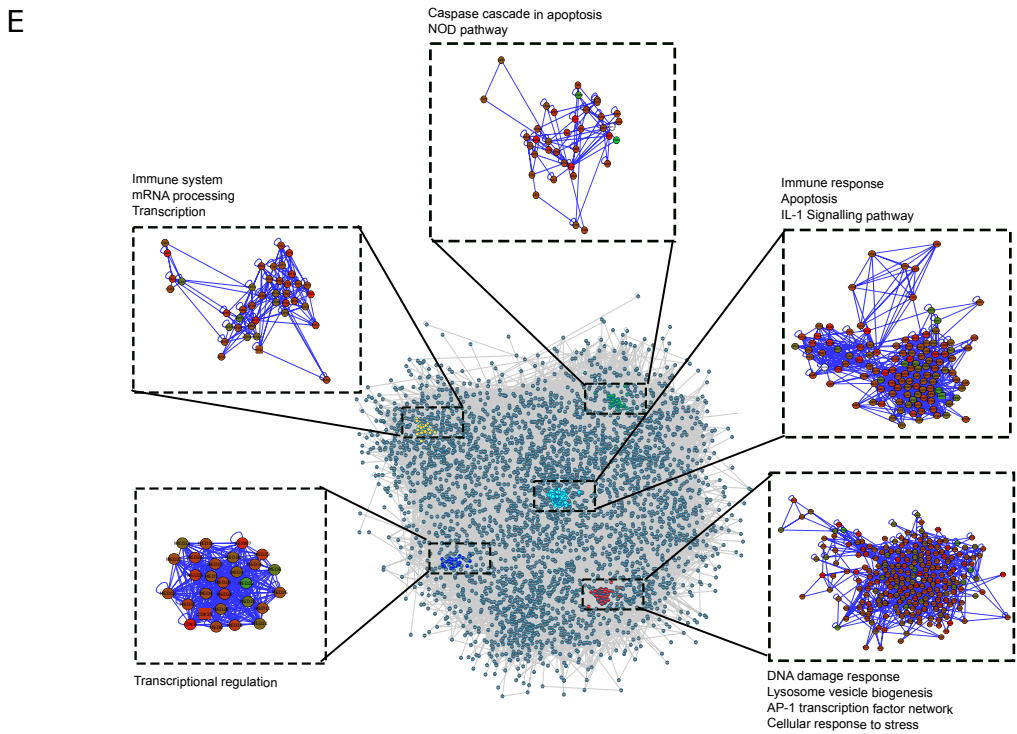
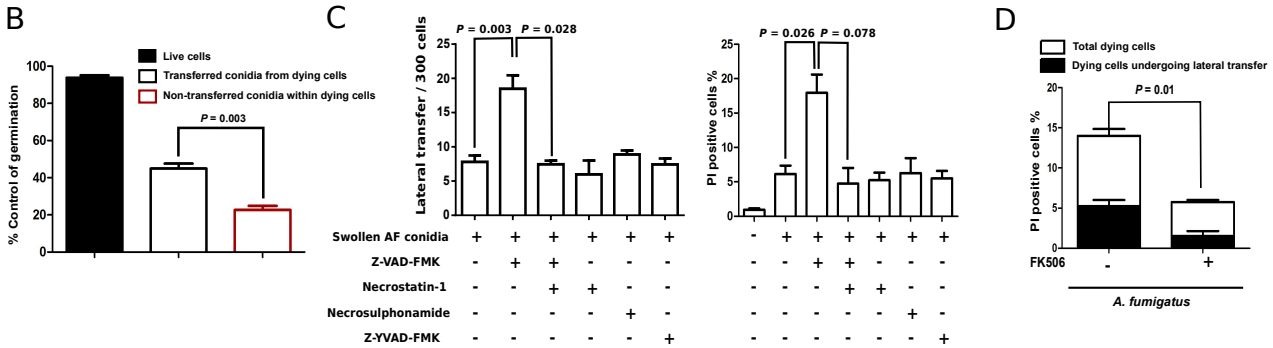
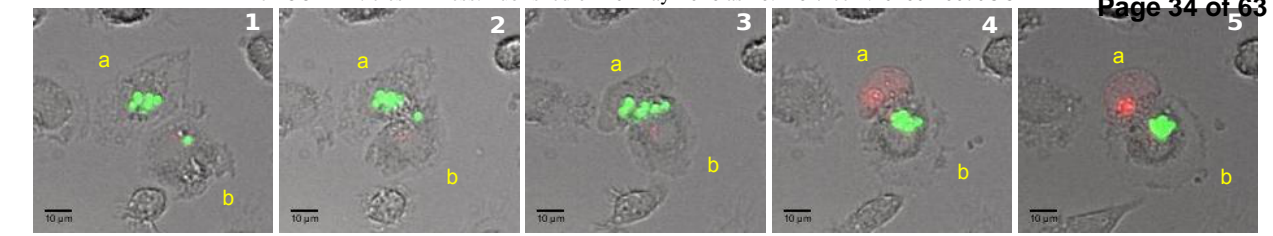
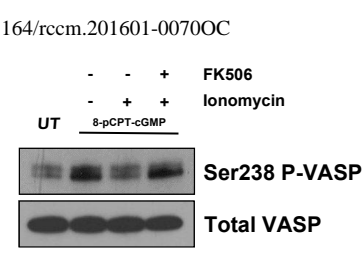


Figure 2. Human macrophage phagocytosis, reactive oxygen species production and control of *A. fumigatus* growth are calcineurin dependent

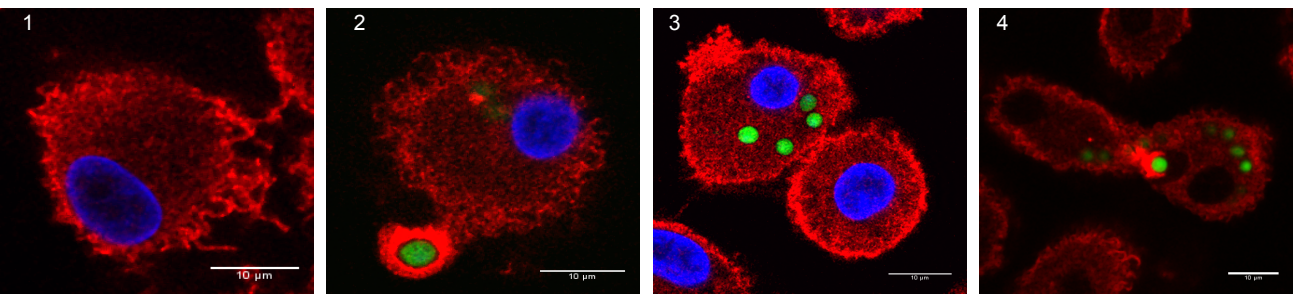




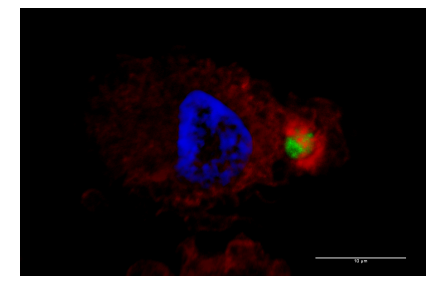
Pathway	Protein	Fold change in phosphoprotein to phosphoprotein in FK506 treated vs Control
Calcineurin/NFAT pathway	AKT1 (Phospho-Ser124)	0.45
	Calmodulin (Phospho-Thr79/Ser81)	0.13
Actin cytoskeleton	VASP (Phospho-Ser238)	26.70
Cell-cycle regulation	CDC25A (Phospho-Ser75)	3.82
	p27Kip1 (Phospho-Ser10)	0.44
	SMC1 (Phospho-Ser957)	0.49
	HDAC1 (Phospho-Ser421)	0.49
MAPK pathway	c-Jun (Phospho-Tyr170)	2.20
	MEK1 (Phospho-Ser298)	2.69
	P90RSK (Phospho-Thr359/Ser363)	0.44
Angiogenesis	VEGFR2 (Phospho-Tyr1175)	0.47



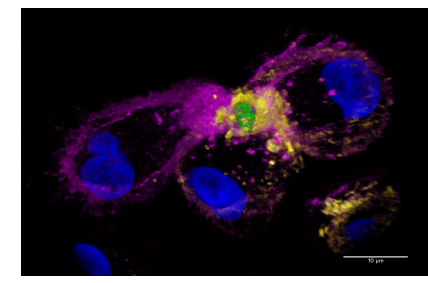
C



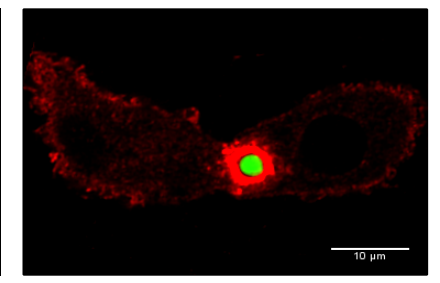
D



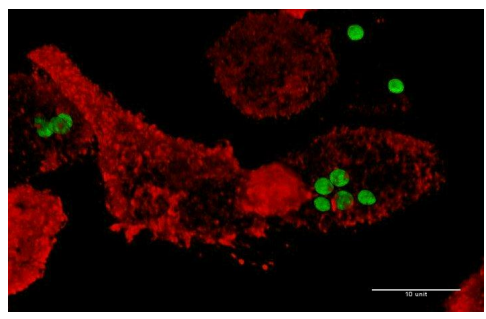
E



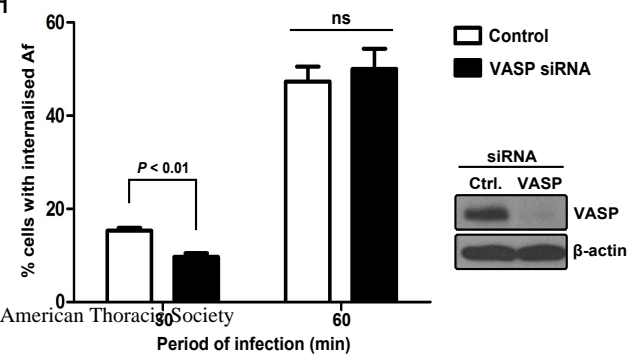
F



G



H



## Movie Legends

**Movie 1. Human monocyte-derived macrophages infected with swollen *A. fumigatus* undergo lateral transfer.**

Representative time-lapse widefield microscopy images of *Af* lateral transfer in human MDMs infected with live *Af* SC (MOI=1, shown in green). Lateral transfer highlighted with black arrow. Images taken at 10 minute intervals.

**Movie 2. Human alveolar macrophages infected with swollen *A. fumigatus* undergo lateral transfer.**

Representative time-lapse widefield microscopy images of *Af* lateral transfer in human AMs infected with live *Af* SC (MOI=1, shown in green). Lateral transfer highlighted with black arrow. Images taken at 10 minute intervals.

**Movie 3. *In vivo* confirmation of macrophage lateral transfer in zebrafish macrophages infected with swollen *A. fumigatus*.**

MPEG:mCherry Zebrafish larvae were infected with ~50 eGFP-expressing conidia of *Af* and time-lapse confocal microscopy performed. Representative three-dimensional reconstructed images show *Af* lateral transfer between macrophages. The transfer process is highlighted with a yellow arrow. Images shown are at 7 minute intervals.

**Movie 4. Macrophages infected with germinating *A. fumigatus* conidia undergo lateral transfer during programmed cell death.**

Representative time-lapse confocal microscopy images of lateral transfer of live *Af* SC (shown in green) between MDMs. Propidium iodide staining (red) showing cell death of macrophage transferring *Af* conidia to neighbouring macrophage. Transfer process highlighted by black arrow. Images taken at 10 minute intervals.

**Movie 5. Massive vacuole formation occurs during *A. fumigatus* germination in human monocyte-derived macrophages**

Representative time-lapse widefield microscopy images of vacuole formation in human MDMs infected with live *Af* SC (MOI=1, shown in green). Images taken at 10 minute intervals.

**Movie 6. VASP co-localises to the human monocyte-derived macrophage *A. fumigatus* phagocytic cup.**

3D reconstruction of confocal microscopy image of phagocytosis of live *Af* SC (MOI=1) by hMDMs. Image of *Af* phagocytosis at 30min p.i. with VASP shown in red, *Af* in green and nuclei in blue.

**Movie 7. Lateral transfer of germinating *A. fumigatus* conidia between human monocyte-derived macrophages occurs within VASP-enveloped endosomes.**

3D reconstruction of confocal microscopy image of hMDM *Af* lateral transfer with VASP shown in green and *Af* in magenta.

**Calcineurin orchestrates lateral transfer of *Aspergillus fumigatus* during macrophage cell death**

Anand Shah, Shichina Kannambath, Susanne Herbst, Andrew Roger, Simona Soresi, Martin Carby, Anna Reed, Serge Mostowy, Matthew C. Fisher, Sunil Shaunak, Darius Armstrong-James

**Online Data Supplement**

## Supplementary Experimental Procedures

### Zebrafish care and maintenance

All zebrafish experiments were approved by the United Kingdom Home Office and performed in accordance with the project license PPL 70/7446. Wild-type adult breeders were purchased from the Zebrafish International Resource Center (Eugene, OR). The Tg(UAS-E1b:Eco.NfsB.mCherry)c24 (referred to as mpeg:mCherry) zebrafish lines have been described elsewhere (1). Embryos were raised in Petri dishes containing 0.5 × E2 medium supplemented with 0.3 µg/ml of methylene blue. For imaging studies, from 24 h post-fertilization (hpf), 0.003% 1-phenyl-2-thiourea (Sigma-Aldrich) was added to the medium to prevent melanin synthesis. Embryos were reared at 30°C, and larvae were anaesthetized with 200 µg/ml tricaine (Sigma-Aldrich) during the injection and imaging procedures

### Fungal strains and culture

*Aspergillus fumigatus* AFCEA10 was used for the Western blot, Luminex, fungal burden, Imagestream, phosphoproteomic and RNA sequencing experiments. An eGFP-expressing strain (ATCC46645-eGFP, a gift from Frank Ebel) was used for all microscopy experiments. All strains were cultured on Sabouraud dextrose agar (Oxoid). Conidia were harvested in 0.1% Tween/H<sub>2</sub>O and filtered through MIRACLOTH (Calbiochem, UK). Conidial suspensions were washed twice in phosphate-buffered saline (PBS) and resuspended in RPMI (Sigma) at concentrations shown. To generate swollen conidia (SC), resting conidia (RC) were suspended in RPMI at  $1 \times 10^6$  conidia/ml and swollen at 37°C for 4 h. Fixed SC were generated by fixing in 2% formalin for 30 min at 4°C, followed by quenching in 0.1M ammonium chloride for 10 minutes and further washes in PBS x4.

**Isolation of human alveolar macrophages**

A total of 240 ml saline bronchoalveolar lavage (BAL) was performed by flexible bronchoscopy and return transferred on ice for processing. BAL fluid was passed through a 100µm cell strainer (BD Bioscience, UK) and centrifuged at 400g for 10 min to pellet cells, which were subsequently washed in cold PBS and resuspended in pre-warmed RPMI 1640. Macrophages were plated at the desired concentration and adhered for 1hour. These purified AMs were then further rested for 3 days to ensure any residual calcineurin inhibitor effect was removed.

**Isolation of monocyte-derived macrophages**

Peripheral blood mononuclear cells (PBMCs) were isolated from 60 ml of healthy volunteer blood or from leukocyte cones purchased from the National Blood Service, Colindale, UK by mixing 3:1 in warm RPMI and layering over Ficoll-Paque plus (GE healthcare) and centrifuging at 450g for 45 minutes. PBMCs were washed at 200g in cold PBS to remove platelets and monocytes subsequently purified by negative magnetic bead selection using a pan-monocyte isolation kit (Miltenyi Biotech, Auburn, CA). To obtain monocyte-derived macrophages (MDMs), freshly isolated monocytes were cultured with RPMI 1640 medium supplemented with 10% human serum (Sigma, UK) and 5 ng/ml granulocyte macrophage colony-stimulating factor (GM-CSF) (Peprotech, UK) for 7 days at 37°C.

**Western blotting**

For whole-cell lysates, cells were lysed in 150 mM NaCl, 50 mM Tris (pH 8), 1% Triton X-100 containing proteinase/phosphatase inhibitor cocktail (Cell Signalling, US). Cytoplasmic and

nuclear extracts were prepared using the NE-PER extraction reagents (Thermo Scientific). Extracts were separated by 4–15% Bis-Tris gel (BioRad), and proteins transferred to PVDF membranes activated with methanol. Membranes were probed with anti-NFATc2 (sc-7296, Santacruz), anti-NF- $\kappa$ B p65 (C22B4), anti-HDAC1 (10E2), anti-Histone H3 (D1H2), anti- $\beta$ -actin (8H10D10), anti-DSCR1 (D6694, Sigma, UK), anti-VASP (9A2), anti-phospho-VASP (Ser239) (3114), anti-SAPK/JNK (9252), anti-phospho-SAPK/JNK (Thr183/Tyr185) (81E11), anti-p38 MAPK (D13E1), anti-phospho-p38 MAPK (Thr180/Tyr182) (D3F9), anti-DRP1 (D6C7) and anti-phospho-DRP1 (Ser637) (GTX5091, Genetex, US) antibodies. All antibodies, where not specified, were from Cell Signalling, US.

#### **Luminex and TNF- $\alpha$ ELISA assay**

MDMs were plated at  $1 \times 10^5$  per well in a 96-well plate and pre-treated with FK506 (10ng/ml, Calbiochem), human Dectin-1 blocking antibody (3 $\mu$ g/ml, R&D Systems), piceatannol (20 $\mu$ M, Cayman Chemical) or vehicle for 1h followed by stimulation with live Af SC (MOI=1) for 6h. Luminex analysis of culture supernatants was performed using the Milliplex human cytokine/chemokine magnetic bead panel kit from Merck Millipore. Supernatants were assayed for TNF- $\alpha$ , GM-CSF, MCP-1, MIP-1 $\alpha$  and MIP-1 $\beta$ . TNF- $\alpha$  production was additionally assayed using a human TNF- $\alpha$  ELISA kit (R&D Systems) according to manufacturer's instructions.

#### **Real-time PCR**

AMs and human MDMs were stimulated with live Af SC (MOI=1) with FK506 or vehicle pre-treatment for 1h. A total of  $5 \times 10^5$  macrophages were lysed in Tri Reagent 1 and 6h after stimulation and whole RNA extracted using TRIzol and purified further using RNAeasy kit

(QIAGEN). RNA was reverse-transcribed using the QuantiTect kit according to the manufacturer's instruction (Qiagen). Fungal burden was analysed by measuring *A. fumigatus* 18S rRNA (GenBank accession number AB008401) by real time PCR as described (2). For RCAN1.4 and TNF- $\alpha$  mRNA expression, RNA was extracted as above from human MDMs stimulated with live Af SC (MOI=1) pre-treated with or without FK506. RCAN1.4 expression was measured using the primer set, forward primer 5'-AGAAAGCAAGATGCATTTAGAAAC-3' and reverse primer 5'-CGCTGAAGATATCACTGTTTGC-3', and TNF- $\alpha$  was measured using forward primer 5'-CGAGTGACAAGCCTGTAGCC-3' and reverse primer 5'-TTGAAGAGGACCTGGGAGTAG-3'. mRNA expression was normalised to  $\beta$ -actin.

#### Macrophage flow cytometry phenotyping

AMs were harvested at D3 after isolation and MDMs at D7 after differentiation and stained with Zombie-aqua cell viability stain (Biolegend, UK) as per manufacturer's guidelines. Prior to fixation, cells were blocked on ice for 20mins with human FcR block (1 in 100 dilution in PBS/0.1%BSA, BD Biosciences) and subsequently stained with antibodies against CD11b, CD11c, CD206, CD86, HLA-DR, and Dectin-1 for 30mins at RT in the dark (see table below). All antibodies were from Biolegend, UK. Cells were washed with PBS/0.1%BSA x1, fixed as above and then acquired on a Fortessa flow cytometer. Results were analysed using Flow Jo (Oregon, US).

Antibody description	Manufacturer	Clone
anti-CD11b-PerCP/Cy5.5	Biolegend	ICRF44
anti-CD11c-PE/Cy7	Biolegend	3.9
anti-CD206-AF647	Biolegend	15-2

<b>anti-CD86-Brilliant violet 605</b>	<b>Biolegend</b>	<b>IT2.2</b>
<b>anti-HLA-DR-APC/Cy7</b>	<b>Biolegend</b>	<b>L234</b>
<b>anti-Dectin-1-PE</b>	<b>Biolegend</b>	<b>15E.2</b>

### **Imagestream analysis of phagocytosis**

5 x 10<sup>5</sup> MDMs pre-treated with FK506 (10ng/ml) and/or cytochalasin D (5μM, Sigma) for 1h were stimulated with live Af SC (MOI=1) pre-stained with Calcofluor White (Sigma). Infections were synchronised by incubating cells at 4°C for 30min pre and post-infection before starting the experiment by incubation at 37°C. At specified time-points, macrophages were washed twice with warm PBS to remove non-internalised Af conidia. Cells were harvested by incubation with ice-cold PBS and repeat pipetting and centrifugation at 400 x g for 10 minutes. Cells were stained with nuclear stain DRAQ5 (Cell signalling) and fixed with 2% paraformaldehyde. Fixed cells were run on ImageStreamX (Amnis) and data analysed using IDEAS software. Single cells with in-focus nuclei were chosen for analysis and percentage of macrophages with internalised conidial quantified according to Calcofluor White fluorescence within the cell.

### **Reactive oxygen species (ROS) production analysis**

MDMs were plated at 1x10<sup>5</sup>/well in 96-well TC-treated black clear bottom plates (Fisher Scientific). Cells were pre-treated with 10 ng/ml FK506 and 5μM cytochalasin D for 1h and stimulated with live Af SC (MOI=1). Infections were synchronised by centrifugation at 1000rpm for 5 min. 10μM dihydrorhodamine 123 (Life technologies) was added to each well and the reactive oxygen species production measured over 24h using a fluorescent plate

reader (Tecan). For analysis of mitochondrial ROS production, MDMs were plated at  $5 \times 10^5$ /well in 24-well plates and infected with live Af SC (MOI=1) following pre-loading with Mitotracker Orange CM-H2TMRos (Invitrogen) according to the manufacturer's instructions and pre-treatment with FK506 (10ng/ml), or vehicle, for 1h. Cells were harvested at the required time-points using ice-cold PBS/5mM EDTA and fluorescence quantified by flow cytometry (Fortessa). Results were analysed using Flow Jo (Oregon, US).

### **Confocal and time-lapse video microscopy for *in vitro* studies**

For confocal microscopy, cells seeded on coverslips were fixed in 2% PFA for 15 minutes followed by quenching in 50mM  $\text{NH}_4\text{Cl}$  for 10 min. Cells were blocked and permeabilised in PBS containing 10% goat serum (Sigma, UK) and 0.1% Saponin (Sigma, UK) for 2h at room temperature and incubated overnight at 4°C with a primary antibody (anti-NFATc1, clone 7A6, BD Biosciences; anti-Rab 5, clone C8B1, Cell signalling; anti-Rab 7, clone D95F2, Cell Signalling; anti-LAMP-1, clone H4A3, Biolegend; anti-VASP, clone 9A2, Cell Signalling) in blocking buffer. After washing with PBS, cells were incubated with an anti-rabbit AF555 (Life Technologies), anti-rabbit Cy5 or anti-mouse Cy5 antibody with or without Phalloidin AF555 or AF643 (Life Technologies) for 45min at room temperature in the dark and mounted with Vectashield mounting medium containing DAPI (Vector laboratories). Imaging of activated Cathepsin B and phagosomal acidification was performed on live cells using a Magic Red Cathepsin B staining kit (Immunochemistry Technologies) and with MDMs pre-stained using 1 $\mu\text{M}$  LysoTracker Red DND-99 respectively. Colocalisation of acidification, activated Cathepsin B and phagosomal markers was assessed by quantifying the average pixel intensity around single conidia using ImageJ. Live time-lapse imaging was performed by plating human MDMs at  $1 \times 10^5$  cells/well in 8-well  $\mu$ -slides (Ibidi) and stimulating with live

Af SC e-GFP expressing Af, resting Af or fixed Af (MOI=1). Cells were pretreated for 1h with FK506 (10ng/ml, Calbiochem), Bafilomycin (100nM, Sigma), Z-VAD-FMK (50µM, Promega), Necrostatin-1 (10µM, Calbiochem), Necrosulphonamide (5µM, Calbiochem) or vehicle. Following stimulation with Af, propidium iodide was added to the media (1.25µg/ml, Invitrogen) and lateral transfer events visualised by confocal time-lapse imaging using a Leica SP5 inverted confocal microscope. To avoid effects on Af uptake, media was replaced to contain cytochalasin D (5µM, Sigma) and Dynasore (100µM) 1h p.i. and un-internalised conidia removed by washing with warm RPMI x3. Cells were maintained at 37°C with 5% CO<sub>2</sub> during imaging and images analysed using ImageJ with 3D reconstructions performed using Velocity.

### **Electron microscopy**

Human MDMs in 24-well plates were infected with live swollen CEA10 Af conidia (MOI=1). Un-internalised conidia were removed by washing with warm RPMI x3 at 1h p.i., and cultures were subsequently fixed in 2.5% glutaraldehyde in 0.05M cacodylate buffer at 15min intervals from 105min p.i. to 180min p.i.. Samples were post-fixed in 1.0% osmium tetroxide, dehydrated through a methanol series (70-100%) and embedded in epoxy resin. Regions of interest were selected from 1.0 µm thick toluidine blue-stained resin survey sections. Ultrathin sections (70–80 nm) were contrast-stained with uranyl acetate and lead citrate then examined by transmission electron microscope (JEOL 1400+, Jeol Ltd, UK). Digital images were captured using an AMT 16X camera (Deben, UK).

### **Zebrafish infection experiments and imaging**

At 2 days post-fertilization (dpf), zebrafish larvae were transferred into 0.5 × E2. For zebrafish infection studies,  $1 \times 10^8$  resting e-GFP Af conidia were stained overnight at 4°C with Alexa-fluor 488 5-SDP ester (Life Technologies) at 400 µg/ml in 250 µl of 0.1M NaHCO<sub>3</sub> pH 8.3 buffer, washed twice with 0.1% Tween/H<sub>2</sub>O followed by PBS and resuspended in PBS containing 1% polyvinylpyrrolidone (Sigma, UK). At Day 3, up to 10 µl of prestained AF resting conidia from a stock concentration of  $5 \times 10^7$ /ml was injected into the hindbrain resulting in an inoculum of 10 to 50 conidia per embryo. Infected larvae were embedded in 1% agarose in 35mm live-imaging µ-dish (Ibidi) and covered with 0.5 × E2 media. Macrophage recruitment and AF lateral transfer was imaged with live time-lapse imaging in a humidified incubation chamber at 30°C using a Leica SP5 resonant inverted confocal microscope. Images were analysed using ImageJ and Velocity.

### **RNA extraction, RNA library preparation and sequencing**

$5 \times 10^5$  MDMs ( $n = 6$ , healthy donors) were plated in 24 well plates and half of the plates pre-treated with 10 ng/ml FK506 for 1h. Cells were stimulated with live Af SC (MOI=1) for 1h and 6h and total RNA extracted using TRIzol reagent (Life technologies). RNA was further purified using an RNAeasy kit (QIAGEN) with an additional purification step by on-column DNase treatment using the RNase-free DNase Kit (QIAGEN) to ensure elimination of genomic DNA. RNA quality was analysed using a 2200 Tape station (Agilent Technologies). RNA with a RIN greater than 9.0 was used for library preparation. One microgram of total RNA was used to generate RNA-seq libraries using the mRNA seq kit v2 (Illumina, Essex, UK), according to the manufacturer's instructions. Briefly, RNA was purified and fragmented using poly-T oligo-attached magnetic beads using two rounds of purification, followed by the first and second cDNA strand synthesis. Next, cDNA 3' ends were adenylated and

adapters were ligated, followed by 10 cycles of library amplification. Finally, the libraries were selected by size using AMPure XP beads (Beckman Coulter) and purified. Constructed libraries were assessed with a 2200 Tape station and quantified using a KAPA Illumina SYBR Universal Lib QPCR kit (Anachem Ltd, Bedfordshire, UK) and broad range Qubit analysis using the QuantiT dsDNA BR assay (Life technologies). Libraries were then sequenced to generate 150-bp paired-end reads on an Illumina HiSeq 2500 (Genome facility, MRC Clinical Science Centre).

### **Mapping of sequenced reads and differential gene expression analysis**

Quality filtered Illumina paired-end reads were mapped to human reference genome (hg19) using the read alignment software TopHat2 with default parameters (3). Genes that have zero counts across all samples were removed from the dataset. Sequencing and mapping were controlled for quality using standard tools provided in the FastQC software (<http://www.bioinformatics.bbsrc.ac.uk/projects/fastqc>). Differential expression analyses were done with Cufflinks v2.2.1 (4). Genes differentially expressed (DE genes) with FK506 treatment and Af stimulation (at 1h and 6h time points) were identified with 2 fold gene expression changes (both up and down) with less than 5% false discovery rate (FDR). 492 genes were identified with significant differential expression at 6 hours of FK506 treatment. DE genes were used to construct regulatory networks in Cytoscape and STRING v9.05 (5, 6). In Cytoscape the DE genes were mapped onto the BioGrid and IntAct protein-protein network database. Nodes were coloured according to the maximal  $\log_2$  ratio across the time points and placed into functional groups. Gene ontology enrichment, functional classification of genes and KEGG pathway enrichment analysis were carried out using DAVID v6.7 (7). All GO categories over-represented with adjusted *P*-value of <0.05 were

obtained for analysis. The Cytoscape Enrichment Map plugin was used to visualize GO biological processes.

### **PPI network construction and network module analysis**

A human PPI network was constructed from the HIPPIE database and the PPI network for the genes expressed in FK506 pre-treated samples were visualised with Cytoscape (8). The network modules were obtained based on the Molecular Complex Detection (MCODE) analysis using the Cytoscape app. Default parameters (Degree Cutoff: 2, Node Score Cutoff: 0.2, K-Core: 2) were used as the cutoff criteria for network module screening (9). GO term enrichment of network modules with MCODE score >10 above were further analysed using BinGO plugin in cytoscape (10).

### **Phosphoproteomic analysis**

The Phospho Explorer Antibody Microarray was conducted by Full Moon BioSystems Inc (California, USA). Human MDMs were differentiated at  $1 \times 10^7$  cells in 75mm<sup>2</sup> tissue culture flasks. At day 7, cells were stimulated with live Af SC (MOI=1) following pre-treatment for 1h with FK506 (10ng/ml, Calbiochem) or vehicle. At 1h post stimulation, cells were washed (x5) with 10mls ice-cold PBS with protease inhibitor (Cell signalling), and collected by gentle scraping and centrifugation (250g for 10min at 4°C). Cells were frozen at -80°C and transferred to Full Moon Biosystems on dry ice. The array consists of 1,318 phospho-specific antibodies. In brief, proteins were labelled with biotin and placed on pre-blocked microarray slides. After washing, detection of total and phosphorylated proteins was conducted using Cy3-conjugated streptavidin. Expression of phosphorylated proteins was normalized to

corresponding total protein expression. Fold change was calculated as follows: phosphorylation of FK506-treated cells/phosphorylation of untreated cells.

### **siRNA transfection of THP-1 cells and flow cytometry analysis of phagocytosis**

$3 \times 10^5$  THP-1 cells were plated in 24-well plate wells and differentiated with 100ng/ml PMA (phorbol myristate acetate) overnight. The next day, cells were transfected with 50 $\mu$ M Signal Silence human VASP siRNA (Cell signalling) and 6 $\mu$ l HiPerfect siRNA transfection reagent/well according to manufacturers' instructions. Cells were left for 72h before washing away remaining complexes with warm RPMI and performing experiments. Cells were infected with swollen CEA10 conidia pre-stained with Calcofluor White (Sigma) as above. Infections were synchronised at 4°C. At 30min and 1h p.i. uninternalised conidia were washed away with warm RPMI and cells were harvested in ice cold PBS/5mM EDTA, fixed in 2% paraformaldehyde (PFA) and uptake analysed by flow cytometry (Fortessa). Results were analysed using Flow Jo (Oregon, US).

### **Statistical analysis**

Data were presented as mean  $\pm$  SEM and were analyzed using GraphPad Prism software (version 6.0; GraphPad). Significance was determined using a Student's *t* test for unpaired observations; \* $P \leq 0.05$ ; \*\* $P \leq 0.01$ ; \*\*\* $P \leq 0.001$ . If 3 or more groups were compared One-way ANOVA with Bonferroni correction was used.  $P < 0.05$  was considered statistically significant.

**Supplemental Table E1. List of genes involved in human apoptosis pathway that are regulated by calcineurin in hMDMs stimulated with Af at 6 hours p.i.**

Gene	Gene description	log2 fold		
		change	p value	q value
ADRB2	adrenergic, beta-2-, receptor, surface	2.03666	5.00E-05	0.0025039
ANGPTL4	angiotensin-like 4	3.14403	5.00E-05	0.0025039
ARF6	ADP-ribosylation factor 6	1.03967	5.00E-05	0.0025039
BAG5	BCL2-associated athanogene 5	1.09531	0.00015	0.00622643
BMF	Bcl2 modifying factor	-1.63738	5.00E-05	0.0025039
BTG2	BTG family, member 2	1.64023	5.00E-05	0.0025039
CARD6	caspase recruitment domain family, member 6	1.5241	5.00E-05	0.0025039
CEBPB	CCAAT/enhancer binding protein (C/EBP), beta	1.30165	5.00E-05	0.0025039
CSF2	colony stimulating factor 2 (granulocyte-macrophage)	1.3387	5.00E-05	0.0025039
EGLN3	egl nine homolog 3 (C. elegans)	1.77097	5.00E-05	0.0025039
FASTKD5	FAST kinase domains 5	1.66276	5.00E-05	0.0025039
FEM1B	fem-1 homolog b (C. elegans)	1.23424	5.00E-05	0.0025039
FOXO1	forkhead box O1	-1.13244	0.0006	0.0195528

GREM1	G protein-coupled receptor 183	1.57284	5.00E-05	0.0025039
	heat shock 70kDa protein 1A; heat shock 70kDa			
HSPA1B	protein 1B	-1.63925	5.00E-05	0.0025039
IER3	immediate early response 3	1.94819	5.00E-05	0.0025039
IL1A	interleukin 1, alpha	1.19629	5.00E-05	0.0025039
IL7	interleukin 7	1.69211	0.00015	0.00622643
MCL1	myeloid cell leukemia sequence 1 (BCL2-related)	1.20625	0.0001	0.00451116
	monocyte to macrophage differentiation-			
MMD	associated	1.32196	5.00E-05	0.0025039
MOAP1	modulator of apoptosis 1	1.48072	5.00E-05	0.0025039
NLRP3	NLR family, pyrin domain containing 3	1.30533	5.00E-05	0.0025039
NUAK2	NUAK family, SNF1-like kinase, 2	-1.53623	0.00055	0.0180311
OSM	oncostatin M	1.7967	5.00E-05	0.0025039
	pleckstrin homology-like domain, family A,			
PHLDA1	member 1	1.54668	5.00E-05	0.0025039
	pleckstrin homology-like domain, family A,			
PHLDA2	member 2	1.07479	0.0003	0.0112934
PHLPP1	PH domain and leucine rich repeat protein	-1.01121	0.00015	0.00622643

	phosphatase 1			
	phosphoinositide-3-kinase, catalytic, gamma			
PIK3CG	polypeptide	1.15058	0.00015	0.00622643
	phorbol-12-myristate-13-acetate-induced protein			
PMAIP1	1	1.3955	5.00E-05	0.0025039
RNF144B	ring finger protein 144B	-1.06347	5.00E-05	0.0025039
RRAGA	Ras-related GTP binding A	1.08069	5.00E-05	0.0025039
	serpin peptidase inhibitor, clade B (ovalbumin),			
SERPINB2	member 2	1.95908	5.00E-05	0.0025039
	solute carrier family 33 (acetyl-CoA transporter),			
SLC33A1	member 1	1.16431	5.00E-05	0.0025039
	tumor necrosis factor (TNF superfamily, member			
TNF	2)	1.284	0.0002	0.00811673
TRAF4	TNF receptor-associated factor 4	-1.2598	5.00E-05	0.0025039

**References:**

1. Mostowy S, Boucontet L, Mazon Moya MJ, Sirianni A, Boudinot P, Hollinshead M, Cossart P, Herbomel P, Levraud JP, Colucci-Guyon E. The zebrafish as a new model for the in vivo study of shigella flexneri interaction with phagocytes and bacterial autophagy. *PLoS pathogens* 2013;9:e1003588.
2. Werner JL, Metz AE, Horn D, Schoeb TR, Hewitt MM, Schwiebert LM, Faro-Trindade I, Brown GD, Steele C. Requisite role for the dectin-1 beta-glucan receptor in pulmonary defense against aspergillus fumigatus. *Journal of immunology* 2009;182:4938-4946.
3. Kim D, Pertea G, Trapnell C, Pimentel H, Kelley R, Salzberg SL. TopHat2: Accurate alignment of transcriptomes in the presence of insertions, deletions and gene fusions. *Genome biology* 2013;14:R36.
4. Trapnell C, Roberts A, Goff L, Pertea G, Kim D, Kelley DR, Pimentel H, Salzberg SL, Rinn JL, Pachter L. Differential gene and transcript expression analysis of rna-seq experiments with tophat and cufflinks. *Nature protocols* 2012;7:562-578.
5. Cline MS, Smoot M, Cerami E, Kuchinsky A, Landys N, Workman C, Christmas R, Avila-Campilo I, Creech M, Gross B, Hanspers K, Isserlin R, Kelley R, Killcoyne S, Lotia S, Maere S, Morris J, Ono K, Pavlovic V, Pico AR, Vailaya A, Wang PL, Adler A, Conklin BR, Hood L, Kuiper M, Sander C, Schmulevich I, Schwikowski B, Warner GJ, Ideker T, Bader GD. Integration of biological networks and gene expression data using cytoscape. *Nature protocols* 2007;2:2366-2382.
6. Jensen LJ, Kuhn M, Stark M, Chaffron S, Creevey C, Muller J, Doerks T, Julien P, Roth A, Simonovic M, Bork P, von Mering C. String 8-a global view on proteins and their functional interactions in 630 organisms. *Nucleic acids research* 2009;37:D412-D416.
7. Dennis G, Jr., Sherman BT, Hosack DA, Yang J, Gao W, Lane HC, Lempicki RA. David: Database for annotation, visualization, and integrated discovery. *Genome biology* 2003;4:P3.
8. Schaefer MH, Fontaine JF, Vinayagam A, Porras P, Wanker EE, Andrade-Navarro MA. Hippie: Integrating protein interaction networks with experiment based quality scores. *PloS one* 2012;7.
9. Bader GD, Hogue CW. An automated method for finding molecular complexes in large protein interaction networks. *BMC bioinformatics* 2003;4:2.
10. Maere S, Heymans K, Kuiper M. Bingo: A cytoscape plugin to assess overrepresentation of gene ontology categories in biological networks. *Bioinformatics* 2005;21:3448-3449.

**Figure E1. FK506 inhibits *A. fumigatus* mediated activation of the calcineurin/NFAT pathway in human lung transplant alveolar macrophages and healthy monocyte-derived macrophages.**

(A) MDMs were stimulated with live *Af* SC (MOI=1) and macrophage nuclear extracts probed by western blot for NFATc1. NFATc1 was normalised to HDAC1 and nuclear translocation quantified. N =3

(B) AMs isolated from human lung transplant recipients after bronchoscopy were stimulated with live *Af* RC (MOI=1) and macrophage nuclear extracts probed by western blot for NFATc2. N =5

(C) MDMs were stimulated with live *Af* RC (MOI=1) and total RNA extracted at various time points p.i. mRNA expression of the NFAT-specific regulatory target RCAN1.4 was normalised with  $\beta$ -actin and quantified. N =5

(D) AMs isolated from human lung transplant recipients after bronchoscopy were stimulated with live *Af* SC (MOI=1) and macrophage nuclear extracts probed by western blot for NFATc2. N =5

(E) MDMs pre-treated with FK506 (10ng/ml) or vehicle were stimulated with live *Af* SC (MOI=1) macrophage nuclear extracts probed by western blot for NFATc1. NFATc1 nuclear translocation was normalised with HDAC1 and quantified. N =4

(F) MDMs pre-treated with FK506 (10ng/ml), NF- $\kappa$ B inhibitor SC514 (10  $\mu$ M) or vehicle were stimulated with live *Af* SC (MOI=1) and total RNA was extracted at various time point p.i. mRNA expression of the NFAT-specific regulatory target RCAN1.4 was normalised with  $\beta$ -actin and quantified. N =5

(G) TNF- $\alpha$  mRNA expression quantified from total RNA isolated from MDMs infected with live *Af* SC (MOI=1) and pre-treated with FK506 (10ng/ml) or vehicle. N =4

(H) Healthy hMDMs (N=4) and AMs (N=5) isolated from lung transplant recipients were characterised by flow cytometry. Cells were gated on live-dead stain<sup>-</sup>, forward and size scatter and CD45<sup>+</sup>. Both healthy MDMs and lung transplant AMs are CD11c<sup>+</sup>, MHC<sup>+</sup> and CD206<sup>+</sup>. MDMs are CD11b<sup>+</sup> whereas AMs are CD11b<sup>-</sup>.

(I-J) TNF- $\alpha$  production measured by ELISA and NFATc1 nuclear translocation was analysed by confocal microscopy shown in MDMs pre-treated with Dectin-1 blocking monoclonal antibody (3 $\mu$ g/ml) or the Syk inhibitor piceatannol (20 $\mu$ M) and infected with live *Af* SC (MOI=1). N=4. Data are represented as mean  $\pm$  SEM

**Figure E2. Calcineurin inhibition leads to impaired phagocytosis and ROS production in human macrophages infected with *Aspergillus fumigatus* but does not affect phagosomal maturation.**

(A) AMs isolated from human lung transplant recipients after bronchoscopy were pre-treated with FK506 (10ng/ml) or vehicle and stimulated with live *Af* SC (MOI=1). Total RNA was isolated at 1 and 6 hour p.i. Fungal growth was assayed by RT-PCR of fungal RNA. N =5

(B) MDMs pre-treated with FK506 (10ng/ml) or cytochalasin D (5nM) or vehicle were stimulated with live *Af* RC (MOI=1) and pre-stained with Calcofluor white. N =3

(C) AMs isolated from human lung transplant recipients after bronchoscopy were pre-treated with FK506 (10ng/ml), Cytochalasin D (5nM) or vehicle and stimulated with live *Af*

SC (MOI=1). *Af* SC (pre-stained with Calcofluor White) phagocytosis by AMs (pre-stained with Draq5, Abcam) were quantified using Imagestream. N =6

(D) MDMs pre-treated with FK506 (10ng/ml) or vehicle were stimulated with live *Af* RC (MOI=1) and ROS production assayed by luminescence. N=4

(E) MDMs stained with Mitotracker Orange CM-H2TMRos (Invitrogen) were pre-treated with FK506 (10ng/ml) or vehicle and stimulated with live *Af* SC (MOI=1). Cells were analysed at 0, 2 and 4h p.i. by flow cytometry and fluorescence quantified by Flow Jo (Oregon, US). N=3

(F) MDMs pre-treated with FK506 (10ng/ml) or vehicle were stimulated with live *Af* SC (MOI=1) and LAMP-1 expression analysed by confocal microscopy at 30minute intervals. Phagosomal LAMP-1 intensity was quantified by *ImageJ*. N=3

(G) Representative confocal microscopy image showing LAMP-1 recruitment to *Af* conidia containing phagosomes in MDMs. LAMP-1 is shown in red, nuclei in blue and *Af* in green.

(H) Representative confocal microscopy image showing acidification in *Af* conidia containing phagosomes in MDMs. LysoTracker Red can be seen in red, and *Af* in green.

(I) MDMs stained with LysoTracker Red (Invitrogen) and pre-treated with FK506 (10ng/ml) or vehicle were stimulated with live *Af* SC (MOI=1) and fluorescence assayed by live confocal microscopy with phagosomal intensity quantified by *ImageJ*. N=3

Data are represented as mean  $\pm$  SEM

**Figure E3. Characterisation of calcineurin-dependent lateral transfer and programmed necrosis in human macrophages infected with *Aspergillus fumigatus*.**

(A) MDMs were stimulated with eGFP live *Af* SC (MOI=1) and treated with Dynasore (100 $\mu$ M) or vehicle following phagocytosis. Fungal burden was quantified by analysis of eGFP fluorescence over time during time-lapse confocal microscopy.

(B) Representative electron microscopy image showing two conidia (indicated by red arrows) contained within specialised compartments being transferred between macrophages.

(C) Phagosomal intensity of maturation markers (Rab5, Rab7 and LAMP-1) assayed by confocal microscopy in MDMs infected with live *Af* SC undergoing lateral transfer and 30 p.i. was quantified by *ImageJ*. N=3

(D) Time-lapse confocal microscopy was performed of human MDMs infected with live SC (MOI=1). Propidium iodide was used to analyse cell necrosis. The conidial area ( $\mu\text{m}^2$ ) as a marker of fungal germination was quantified within cells undergoing programmed necrosis and surrounding live cells. Conidia that undergo lateral transfer are highlighted in red. N=14

(E-F) Time-lapse widefield microscopy images (E) and representative transmission electron microscopy images (F) showing vacuole development in *Af* containing compartments in macrophages infected with live *Af* SC. Electron microscopy image was taken at 180min p.i.. Conidia are indicated by red arrows. Widefield microscopy images taken from 45min p.i. and subsequently at 45min intervals. (See Movie 4)

(G) Quantification of vacuolar development and lateral transfer in MDMs pre-treated with Bafilomycin (100nM) and infected with eGFP live *Af* SC (MOI=1). N=3

(H) MDMs pre-treated with a pan-caspase inhibitor (Z-VAD-FMK 50 $\mu$ M), RIPK-1 inhibitor (Necrostatin-1 10 $\mu$ M), both or vehicle were stimulated with eGFP live *Af* SC (MOI=1) and fungal burden was quantified by analysis of eGFP fluorescence over time. N=3

(I-J) MDMs pre-treated with FK506 (10ng/ml) or vehicle were stimulated with eGFP-expressing live *Af* SC (MOI=1) and time-lapse confocal microscopy performed. Fungal burden was quantified by eGFP fluorescence quantification over time (I) and average conidial size 6h p.i. quantified to assess fungal germination (J). N=4

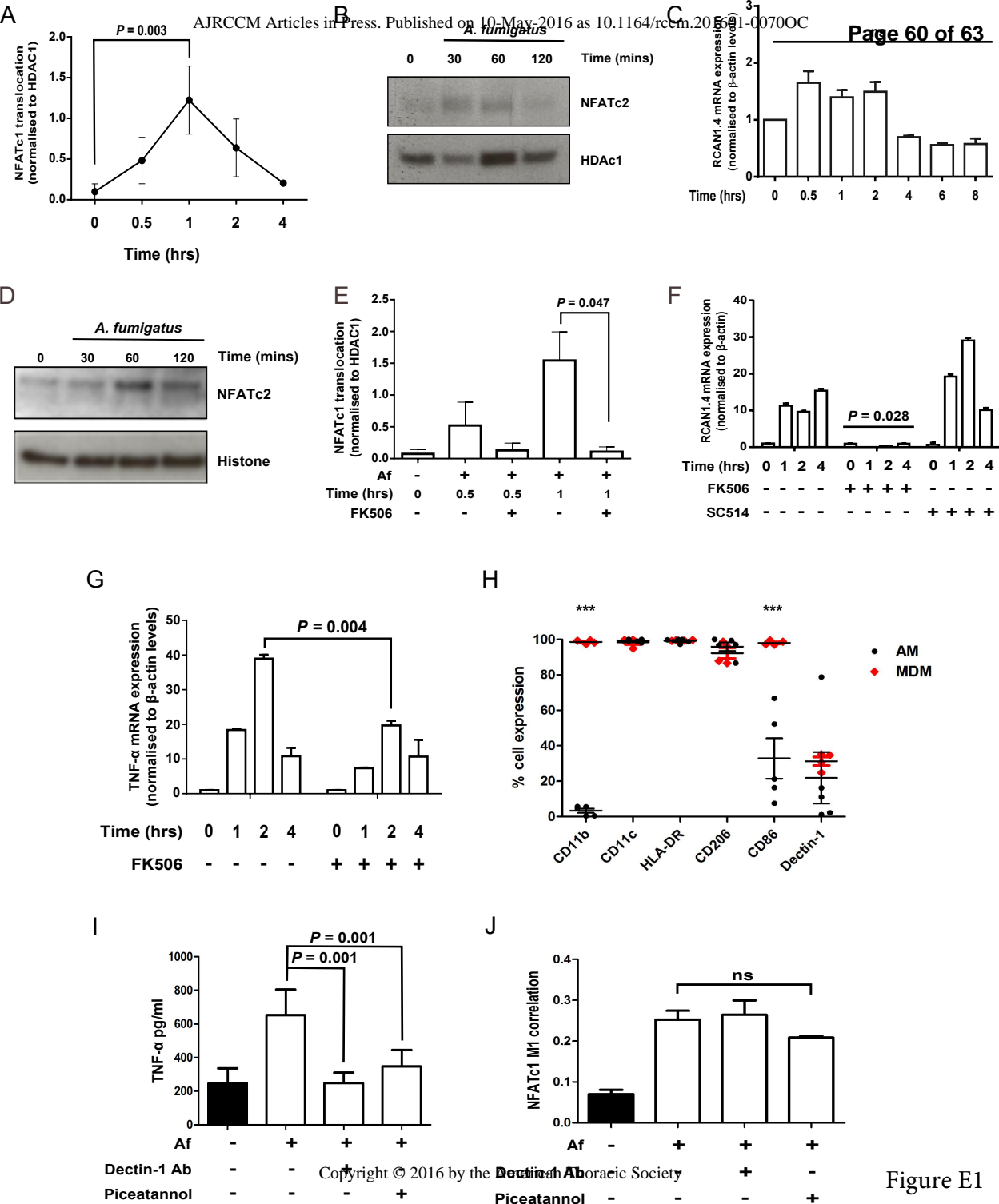
**Figure E4. Transcriptome analysis of FK506 pre-treated monocyte-derived macrophages in response to live *A. fumigatus* infection.**

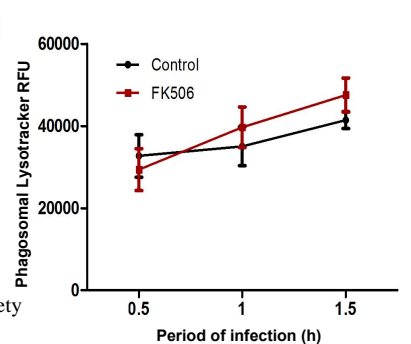
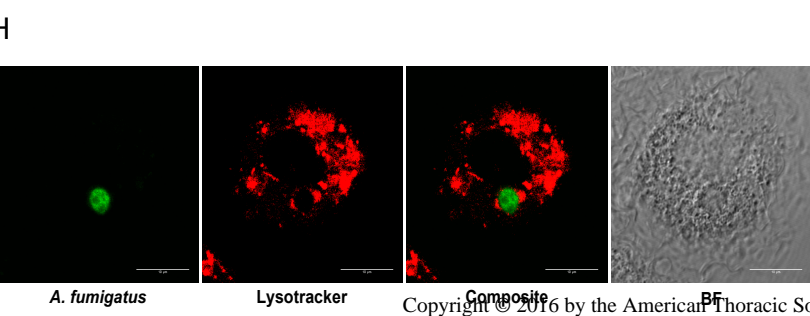
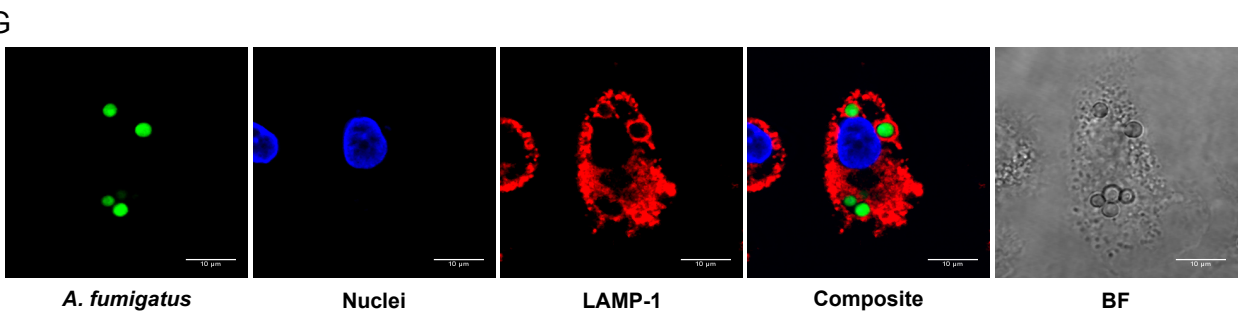
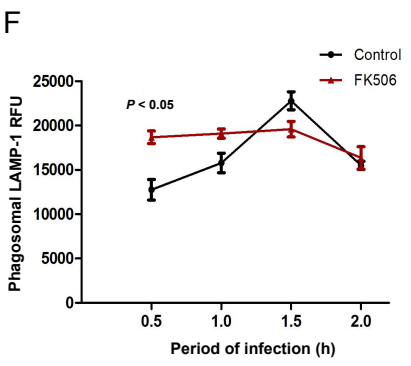
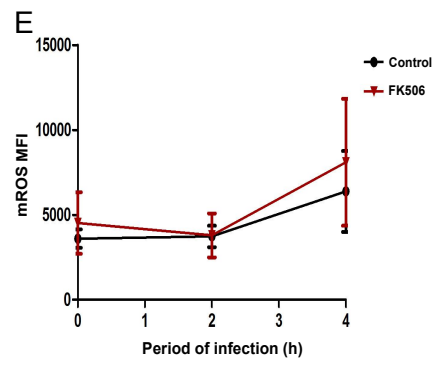
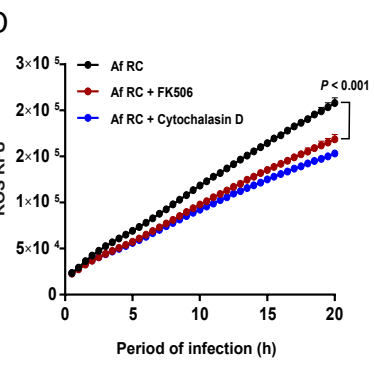
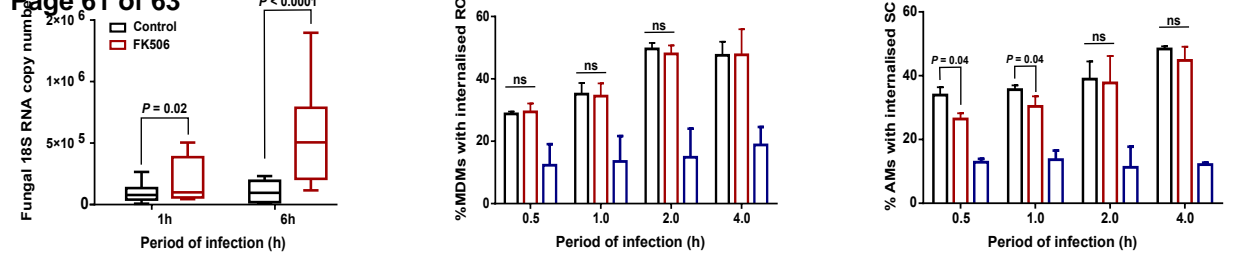
(A) Venn diagram indicating the number of significantly regulated genes after FK506 (10ng/ml) pre-treatment of macrophages stimulated with live *Af* SC (MOI=1). Results shown for 1 and 6 hours together with the overlap between each set of genes.

(B) Selected GO enrichment terms for the differentially expressed genes in MDMs pre-treated after FK506 (10ng/ml) and stimulated with live *Af* SC (MOI=1) for 6 hours. Differentially expressed genes were analysed using the functional annotation tool in DAVID.

(C) Visualisation of selected over represented pathways of differentially expressed genes analysed using ConsensusPathDB (CPDB) interaction map. The node size reflects the total number of components in a pathway; the node colour reflects the p-value of the pathway representation analysis with a darker colour corresponding to a lower p-value.

(D) Monocyte-derived macrophages pre-treated with FK506 (10ng/ml) or vehicle were stimulated with live *Af* SC (MOI=1) and whole cell lysates probed by western blot for DRP-1 phosphorylation and MAPK pathway activation.





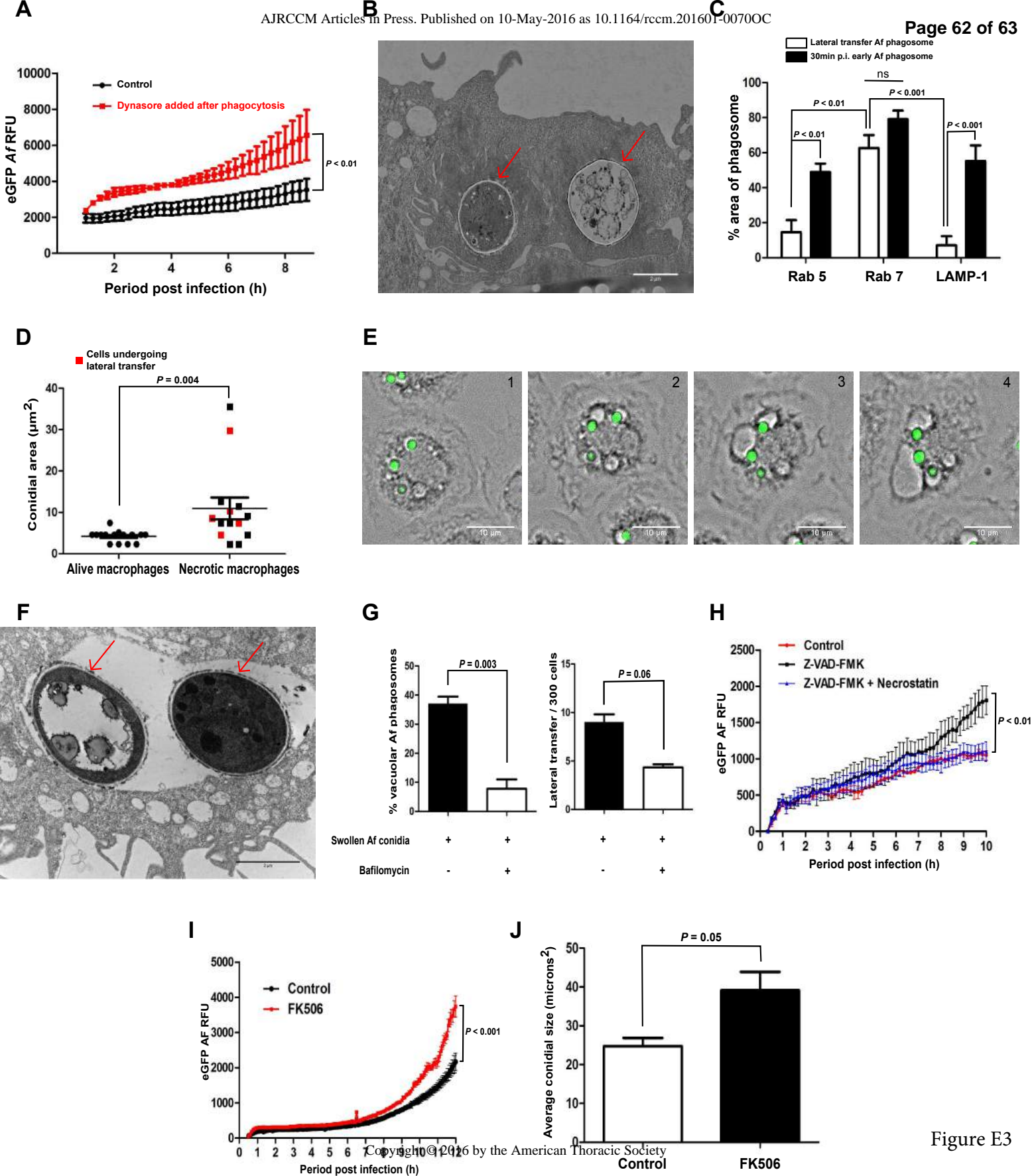


Figure E3

